The School of Mathematics

THE UNIVERSITY
of EDINBURGH

Can we do something useful with a Koopman decomposition?

by

Jiaming Zhang

Dissertation Presented for the Degree of
MSc in Computational Applied Mathematics

August 2022

Supervised by
Jacob Page

Abstract

In this project, the Koopman mode decomposition (KMD) [15, 18] is discussed. The basic definitions and properties of the KMD are recalled, together with the connection between KMD and Dynamic mode decomposition(DMD)[21]. We also demonstrate the KMD on a non-linear dynamical system via near-identity transformation. The finite collections of the eigenfunctions from the linearised system can span and form the Koopman invariant subspace. Then, we define the exact DMD algorithm and present some examples with numerical methods for Koopman analysis. We find a correlation between the largest absolute eigenvalue and the timestep between pairs of snapshots that reduce the error between the exact and DMD eigenvalues. Finally, we present three methods of solving the Burgers equation and apply DMD with different observables on the analytic solutions in both Dirichlet and periodic boundary condition. We demonstrated the complete Koopman analysis of the Burgers equation in different boundary conditions to examine the DMD-Koopman operator connection in practical. We compare the DMD eigenvalues and Koopman eigenvalues and discuss how "far away" should we take the data matrix for DMD be from the simple invariant solution of the Burgers equation to perform the first few accurate DMD eigenvalues with different initial and boundary conditions.

Acknowledgements

I want to thank my supervisor, Dr Jacob Page, for their consistent, enthusiastic support and comprehensive feedback on my work, from the project's beginning to the finish.

Own Work Declaration

I declare that this thesis was composed by myself and that the work contained therein is my own, except where explicitly stated otherwise in the text.

Contents

1 Introduction **1**
- 1.1 Background and Motivation . . . 1
- 1.2 Thesis Contribution . . . 2
- 1.3 Outline of Thesis . . . 2

2 Definitions in Dynamical Systems **3**
- 2.1 Dynamical Systems and Flows . . . 3
- 2.2 Solution of the Linear Problem . . . 4

3 Koopman Operator Theory **5**
- 3.1 General Definitions in Koopman Theory . . . 5
- 3.2 Koopman Eigenfunctions . . . 5
- 3.3 Koopman Mode Decomposition . . . 7
  - 3.3.1 Koopman Mode Decomposition in Linear System . . . 8
  - 3.3.2 Koopman Mode Decomposition in Non-linear System . . . 10
  - 3.3.3 Detailed Analysis of a Simple Non-linear System . . . 11
  - 3.3.4 Determine Eigen-pairs by Solving the governing PDE . . . 16

4 Numerical Methods for Koopman Mode Analysis **18**
- 4.1 Dynamic Mode Decomposition . . . 19
- 4.2 Koopman Spectral Analysis . . . 21

5 Burgers Equation **27**
- 5.1 Cole-Hopf Transformation . . . 27
- 5.2 Solve Burgers Equation via Finite difference . . . 28
- 5.3 Solve Burgers Equation via Fourier series . . . 29
- 5.4 Solve Burgers Equation via Koopman Mode Decomposition . . . 30
- 5.5 Dynamic Mode Decomposition on Burgers Equation . . . 31
- 5.6 Burgers Equation with Periodic Boundary Condition . . . 34

6 Conclusions **36**

List of Tables

List of Figures

1 A figure of what is the impact of the Koopman operator and the relation to the dynamical system (the graph is modified based on the one from [2]). The top part evolves the state, $\mathbf{x} \in \mathcal{M}$, via the flow map $f^t(\mathbf{x})$. The bottom part evolves the observable, $g : \mathcal{M} \in \mathbb{C}$, via the Koopman operator, $\mathcal{K}^t$. . . 6

2 (a) Phase plane for System 3.39 with $\mu = -0.1$ and $\lambda = -0.5$. The grey lines denote the level sets of the Koopman eigenfunctions $\varphi_\mu(vertical)$ and $\varphi_\lambda(curved)$. The invariant manifolds are represented by the thick lines. (b) Phase portrait with contour plot for System 3.39 with $\mu = -0.1$ and $\lambda = -0.5$.. The red dot in the centre denote the origin, and the grey lines with arrow represent the flow of the system, and the colour is the different levels sets. 11

3 The flow of the observable function against the flow computed by Koopman mode decomposition and the error between the exact flow and the Koopman mode decomposition with the initial point $(1, 1)$ and time $t = 60$ for the non-linear system (3.39). 14

4 The loglog plot for the relative error $\frac{\lambda_{exact}-\lambda_{DMD}}{|\lambda_{exact}|}$ between different values of μ and λ in different Δt that $\Delta t = \text{logspace}[-3, 4]$ 23

5 The loglog plot for the relative error $\frac{\lambda_{exact}-\lambda_{DMD}}{|\lambda_{exact}|}$ and $|\lambda_i|\Delta t$ with $\lambda = -0.05$ and $\mu = -0.1, -0.5, -1, -2, -5$ and -10. 24

6 The loglog plot for the sum of the relative errors $\frac{\lambda_{exact}-\lambda_{DMD}}{|\lambda_{exact}|}$ and the smallest eigenvalue multiply with Δt, $\Delta t = \text{logspace}[-1.5, 1]$ 24

7 The flow of the non-linear system 3.39 against the flow computed by DMD and the error between the exact flow and the DMD with the initial point $(1, 1)$ and time $t = 60$ with $\Delta t = 0.6$ 25

8 The comparison of exact eigenvalues and DMD eigenvalues, with $\mu = -1$ and $\lambda = -0.05$ the blue horizontal line is the real part of the exact eigenvalues, The blue dot is the exact eigenvalues and the red circle is the DMD eigenvalues. (a) We plotted all the exact and DMD eigenvalues. (b) We plotted the part without three outer DMD eigenvalues and the non-repeated exact eigenvalues. 26

9 Evolution of $u_0(x) = \sin\left(\frac{2\pi x}{L}\right)$ for $t \leq 200$, The line is computed by analytic solution, the dot is computed by finite difference method. 28

10 Eigenvalues from DMD of $u_0(x) = \sin\left(\frac{2\pi x}{L}\right)$ with 400 snapshot pairs with timestep $\Delta t = 0.5$, with the time interval $t \in [0, 200]$ for both $\mathbf{g} = \mathbf{u}$ and $\mathbf{g} = \mathbf{v}(\mathbf{u})$. The blue horizontal lines are the eigenvalues of the linear diffusion problem $-\nu\left(\frac{n\pi}{L}\right)^2$. 32

11 First a few eigenvalues from DMD of $u_0(x) = \sin\left(\frac{2\pi x}{L}\right)$ with 20 snapshot pairs with timestep $\Delta t = 0.5$, with the time interval $t \in [190, 200]$ for both $\mathbf{g} = \mathbf{u}$ and $\mathbf{g} = \mathbf{v}(\mathbf{u})$. The blue horizontal lines are the eigenvalues of the linear diffusion problem $-\nu\left(\frac{n\pi}{L}\right)^2$. 33

12 (a): Eigenvalues from DMD of $u_0(x) = \sin\left(\frac{2\pi x}{L}\right)$ with 20 snapshot pairs with timestep $\Delta t = 0.5$, with the time interval $t \in [195, 200]$ for $\mathbf{g} = \mathbf{u}$. (b): First a few eigenvalues from DMD of $u_0(x) = \sin\left(\frac{2\pi x}{L}\right)$ with timestep $\Delta t = 0.5$, collected within the different time intervals between $25, 50, 100, 150, 175, 195$ to 200 for $\mathbf{g} = \mathbf{u}$. 33

13 First a few eigenvalues from DMD of $u_0(x) = \exp[-(x + \left(\frac{\pi}{2}\right)^2)]$ with timestep $\Delta t = 0.5$, with the different time intervals between $25, 50, 100, 150, 175, 195$ to 200 for $\mathbf{g} = \mathbf{u}$. 34

14 (a): Evolution of $u_0(x) = \sin\left(\frac{2\pi x}{L}\right)$ for $t \leq 200$, The line is computed by periodic boundary condition, the dot is computed by Dirichlet boundary condition. (b): First a few eigenvalues from DMD of $u_0(x) = \exp[-(x + \left(\frac{\pi}{2}\right)^2)]$ with timestep $\Delta t = 0.5$, with the different time intervals between $25, 50, 100, 150, 175, 195$ to 200 for $\mathbf{g} = \mathbf{u}$ with periodic boundary condition. 35

1 Introduction

1.1 Background and Motivation

Nonlinearity is a central challenge in dynamical systems, resulting in a wide range of phenomena ranging from bifurcations to chaos and manifesting across multiple disciplines. However, no overarching mathematical framework exists for both explicitly and generally characterising non-linear systems. Many researchers were trying to decompose the state of the non-linear system into a series of spatial decompositions to form a more straightforward state with known time behaviour to predict and control it. In contrast, linear systems are completely characterised by their spectral decomposition (i.e., eigenvalues and eigenvectors), resulting in algorithms for prediction, estimation, and control that are generic and computationally efficient. In 1931, B.O.Koopman[13] demonstrated that using an infinite-dimensional linear operator on the Hilbert space of observable functions can analyse the non-linear dynamical systems associated with Hamiltonian flows. The Koopman operator is an infinite-dimensional linear operator, advancing the system's observable functions, and its spectral decomposition completely characterises the non-linear system's behaviour. The search for tractable finite-dimensional representations of the Koopman operator is closely related to the search for effective coordinate transformations that make non-linear dynamics appear linear. Recently, it was demonstrated that Koopman analysis could generalise the Hartman-Grobman theorem to the entire basin of attraction of a stable or unstable equilibrium point[17].

Through the work of Mezić and Banaszuk([18],[15]), many researchers put much effort into exploring Data-driven Koopman analysis to represent the complex system. We are interested in using the approximations of the finite-rank linear Koopman operator to propagate the original non-linear dynamics. Introducing the Koopman operator can transfer the finite-dimensional non-linear dynamics to the infinite-dimensional linear dynamics. Therefore we can approximate the dynamics by the finite-dimensional linear Koopman operator. A Koopman-invariant subspace is formed by any set of Koopman eigenfunctions, yielding an exact finite-dimensional linear model. However, there is a limitation with it, this only works for a single isolated fixed point dynamical system. It is difficult to determine the eigenfunctions for the state, but as long as we know the Koopman eigenfunction, we can use them to recover the state.

Dynamic mode decomposition (DMD) was proposed by P.Schmid [22] in 2010, providing a practical numerical framework for Koopman mode decomposition that demonstrates a method based on numerical and experimental time series with a fixed spatial structure and exponential time dependence. However, choosing the correct parameters of DMD and observables(measurements) to use for a given non-linear system and how they will impact the performance and accuracy of DMD is still an open problem. DMD is frequently applied to massive dynamical systems with an underlying Partial differential equation(PDE) where we do not know much about the Koopman eigenfunctions in practice. Besides, even if we can find a finite subset of the Koopman eigenfunctions, we can not ensure the state variable is in the span of the Koopman invariant subspace. By taking advantage of the Cole-Hopf transformation([6] [11]), Jacob[20] derive the full Koopman mode decomposition of solutions to the Burgers equation and evaluate the capability of DMD to extract these objects from time series. Nevertheless, the DMD output eigenvalues do not match all the Koopman eigenvalues around the fixed point. It is challenging how we choose the input data matrices into DMD to perform the best results.

In this work, we demonstrated the complete Koopman analysis of the Burgers equation in different boundary conditions to examine the DMD and the Koopman operator connection in practice. We answer the two questions: how we should select the parameters of DMD in a given non-linear system to perform a robust Koopman decomposition

numerically with the best accuracy and how "far away" we are from the simple invariant solution in the Burgers equation.

1.2 Thesis Contribution

This thesis proposes solving non-linear dynamical system and PDEs via KMD. The proof of basic notations and definition is given in Section 3.3 with an example of using KMD to solve a non-linear dynamical system by both numerical and analytical methods. The exact DMD algorithm is carried out in Section 4.1. We also use the proposed DMD algorithm on non-linear dynamical system to determine the relationship between the eigenvalue and timestep with the error of DMD in Section 4.2. We then discussed the data range about the fixed point to have the better result on the eigenvalue of the Burgers equation with the DMD algorithm. Furthermore, we explore the result in Burgers equation with periodic boundary condition. In summary, we demonstrate how to pick a suitable timestep on performing DMD on the data, and how to pick the right data range to perform DMD to receive better result.

1.3 Outline of Thesis

The following sections of the thesis are organised as follows. Chapter 2 consists of basic definitions and theorems in dynamical systems. Chapter 3 provides a practical introduction Koopman operator theory, the Koopman mode decomposition, and spectral theory, by including suitable examples. Chapter 4 introduces Dynamic mode decomposition and its link to Koopman operator, followed by several results. In Chapter 5 the Burgers equation is solved with different methods, by applying Koopman analysis on Burgers equation with several boundary conditions, together with discussions of all results and suggestions for further research in Chapter 6.

2 Definitions in Dynamical Systems

Before summarising recent development in Koopman theory, we first provide a mathematical introduction to basic definitions and theorems in dynamical systems. All the definitions here follow those in the Lecture notes from Jacob Page in the course Applied dynamical system at University of Edinburgh[19].

2.1 Dynamical Systems and Flows

Define a State Space $\mathcal{M} \subset \mathbb{R}^d$. Then the state of the system is denoted by $\mathbf{x} \in \mathcal{M}$. The state depends on the time t, so the evolution of $\mathbf{x}$ with t

$$\dot{\mathbf{x}} \equiv \frac{d\mathbf{x}}{dt} = F(\mathbf{x}, t), \tag{2.1}$$

where $F : \mathcal{M} \to \mathbb{R}^d$ is a vector field on the state space $\mathcal{M}$.

We will often consider autonomous continuous-time dynamical systems

$$\frac{d}{dt}\mathbf{x}(t) = F(\mathbf{x}(t)). \tag{2.2}$$

Similarly, we consider autonomous discrete-time systems

$$\mathbf{x}_{k+1} = f(\mathbf{x}_k), \tag{2.3}$$

where x belong to the state space $\mathcal{M} \subset \mathbb{R}^d$, k is the discrete time index and $f : \mathcal{M} \to \mathcal{M}$ is the *dynamic map*. The discrete-time dynamic systems are more general than the continuous one defined in (2.2), as they include discontinuous and hybrid systems. In fact, discrete-time dynamic systems can be derived from continuous ones by sampling the trajectory in equation (2.2) discretely in time, so that $\mathbf{x}_k = \mathbf{x}(k\Delta t)$. The time step Δt now parameterises the discrete-time propagator f.

Definition 2.1 (Flow)**.** For an arbitrary time $t \in \mathbb{R}$, we define the *flow map* $f^t : \mathcal{M} \to \mathcal{M}$ for the system (2.1) to be the map that takes the initial state to the state at time t, or equivalently

$$f^t(\mathbf{x}(t_0)) = \mathbf{x}(t_0) + \int_{t_0}^{t_0+t} F(\mathbf{x}(\tau))\, d\tau. \tag{2.4}$$

Definition 2.2 (Fixed point)**.** A *fixed point* $x^* \in \mathcal{M}$ is one that satisfies the condition

$$f^t(\mathbf{x}^*) = \mathbf{x}^* \quad \text{or} \quad F(\mathbf{x}^*) = 0 \quad \forall\, t. \tag{2.5}$$

Definition 2.3 (Hyperbolic fixed point)**.** The fixed point x^* of the system $\dot{\mathbf{x}} = F(\mathbf{x})$ is called *hyperbolic* if the Jacobian $DF(\mathbf{x})$ of F at this fixed point has no eigenvalues with zero real part.

Theorem 2.1 (Hartman-Grobman theorem)**.** ([9],[8],[10]) Consider the non-linear dynamical system $\dot{\mathbf{x}} = F(\mathbf{x})$ where $\mathbf{x} \in \mathcal{M}$ with the flow f^t and the linearised system $\frac{d}{dt}(\mathbf{x} - \mathbf{x}^*) = \mathbf{A}(\mathbf{x} - \mathbf{x}^*)$, where $\mathbf{A} = DF(\mathbf{x}^*)$ is the Jacobian of F and $\mathbf{x}^*$ is the hyperbolic fixed point. Then there is a neighbourhood $\mathbb{N}$ of $\mathbf{x}^*$ so that f^t is topologically conjugate to the linear flow associatd with its linearisation $DF(\mathbf{x}^*)$.

Definition 2.4 (Near-identity transformation)**.** Suppose we have a dynamical system in the form

$$\dot{\mathbf{x}} = \mathbf{\Lambda x} + \mathbf{F_2}(\mathbf{x}) + \mathbf{F_3}(\mathbf{x}) + \cdots, \tag{2.6}$$

where Λ is a diagonal matrix with entries are the eigenvalue of the Jacobian of a fixed point $\mathbf{x}^*$, and the terms $\mathbf{F}_r(\mathbf{x})$ contain nonlinearities of degree r, and the near-identity

transformation has the form

$$\mathbf{x} = \boldsymbol{\xi} + \mathbf{h}_r(\boldsymbol{\xi}), \tag{2.7}$$

where $\mathbf{h}_r$ contains nonlinearities of degree r. The transformation is defined as it removed nonlinearities of degree r in the original system.

2.2 Solution of the Linear Problem

A linear dynamical system has the form:

$$\frac{d\mathbf{x}}{dt} = \mathbf{A}\mathbf{x}, \tag{2.8}$$

where $\mathbf{A}$ is a constant square matrix. It is easy to observe that the flow associated with the linear problem (2.8) is

$$f^t(\mathbf{x}) = e^{t\mathbf{A}}\mathbf{x}. \tag{2.9}$$

By using Taylor expansion, we can write the matrix exponential as

$$e^{t\mathbf{A}} := \sum_{n=0}^{\infty} \frac{(t\mathbf{A})^n}{n!}. \tag{2.10}$$

Furthermore, if $\mathbf{A}$ has distinct eigenvalues, we have the following decomposition

$$\mathbf{A} = \mathbf{V}\boldsymbol{\Lambda}\mathbf{V}^{-\mathbf{1}}, \tag{2.11}$$

where V contains the eigenvectors $\mathbf{v}_{\lambda_1}, \mathbf{v}_{\lambda_2}...$ as columns and $\boldsymbol{\Lambda}$ is a diagonal matrix with each diagonal entries as the corresponding eigenvalues, i.e., $\boldsymbol{\Lambda}_{ii} = \lambda_i$. If λ is an eigenvalue of $\mathbf{A}$ with eigenvector $\mathbf{v}_\lambda$, then $\mathbf{v}_\lambda$ is also an eigenvector of $e^{t\mathbf{A}}$ with eigenvalue $e^{t\lambda}$.

We can therefore diagonalise our matrix exponential as

$$e^{t\mathbf{A}} = \mathbf{V}e^{t\boldsymbol{\Lambda}}\mathbf{V}^{-1}, \tag{2.12}$$

where

$$e^{t\boldsymbol{\Lambda}} = \begin{pmatrix} e^{\lambda_1 t} & & \\ & e^{\lambda_2 t} & \\ & & \ddots \end{pmatrix},$$

is a diagonal matrix. The eigenvectors form a good basis for representing the solution to the linear problem $\dot{\mathbf{x}} = \mathbf{A}\mathbf{x}$; if the initial state $\mathbf{x}$ is expanded as

$$\mathbf{x} = \mathbf{V}\mathbf{w} = \sum_{n=1}^{d} w_n \mathbf{v}_{\lambda_n}, \tag{2.13}$$

then we have the representation for the flow map

$$f^t(\mathbf{x}) = e^{t\mathbf{A}}\mathbf{V}\mathbf{w} = \mathbf{V}e^{t\Lambda}\mathbf{w} = \sum_{n=1}^{d} w_n \mathbf{v}_{\lambda_n} e^{\lambda_n t}. \tag{2.14}$$

If we apply a sequence of near-identity transformations, we may remove all the non-linear terms, left with a system of the form $\dot{\boldsymbol{\xi}} = \Lambda\boldsymbol{\xi}$, which satisfies the Hartman-Grobman theorem. But the theorem only holds for a small neighbourhood around the fixed point and in practice we don't know how small is, luckily, Koopman operator can represent a finite-dimensional non-linear system from an infinite-dimensional linear system, and most importantly, we can use near-identity transformation everywhere in the state space.

3 Koopman Operator Theory

3.1 General Definitions in Koopman Theory

The Koopman operator advances observable functions of the state with the flow of the dynamics. We first define a dynamical system (2.2) on a finite-dimensional state space $M \in \mathbb{R}^n$, then we let the initial condition $\mathbf{x}(0)$ flow forward along the time t, so the trajectories evolve are

$$\mathbf{x}(t) = f^t(\mathbf{x}(0)), \tag{3.1}$$

where f^t is the flow map defined in (2.4). The Koopman operator $\mathcal{K}^t$ is a linear operator that defined as:

$$\mathcal{K}^t g = g \circ f^t(\mathbf{x}), \tag{3.2}$$

where $\circ$ is the composition operator and $g : \mathcal{M} \to \mathbb{C}$ is the observable function.

The linearity of the Koopman operator follows from the linearity of the composition operator of the flow map for autonomous dynamical system given in (2.2). That is,

$$\mathcal{K}^t\mathcal{K}^s g(\mathbf{x}) = \mathcal{K}^t g \circ f^s(\mathbf{x}) = g \circ f^t \circ f^s(\mathbf{x}) = g \circ f^{t+s}(\mathbf{x}) = \mathcal{K}^{t+s} g(\mathbf{x}). \tag{3.3}$$

For a discrete-time system $\mathbf{x}_{n+1} = f(\mathbf{x}_n)$, this becomes:

$$\mathcal{K} g(\mathbf{x}_n) = g(f(\mathbf{x}_n)) = g(\mathbf{x}_{n+1}). \tag{3.4}$$

The linearity of $\mathcal{K}$ on the observables follows directly from the defintion, i.e.,

$$\mathcal{K}[g_1 + g_2](\mathbf{x}) = [g_1 + g_2] \circ f(\mathbf{x}) = g_1 \circ f(\mathbf{x}) + g_2 \circ f(\mathbf{x}) = \mathcal{K} g_1(\mathbf{x}) + \mathcal{K} g_2(\mathbf{x}). \tag{3.5}$$

Figure 1 depicts a schematic representation of the Koopman operator. The Koopman operator *lift* the dynamics from the state space to the observables space. The advantage of this is that provides a method of identifying intrinsic coordinate systems where nonlinear dynamics appear to be linear, but the operator is infinite-dimensional, even for linear systems.

3.2 Koopman Eigenfunctions

The Koopman operator is an infinite-dimensional linear operator, posing issues for representation and computation challenges. Koopman analysis attempts to identify basis observable functions that evolve linearly with the flow of the dynamics instead of capturing the evolution of all observable functions in a Hilbert space. The Koopman eigenfunctions provide a set of particular observables that behave linearly in time. The capability to reduce the dynamics through the eigen-decomposition of the operator is a primary motivation for using the Koopman framework.

The observable $\varphi(\mathbf{x}) : \mathcal{M} \to \mathbb{C}$ is defined on the state space has the evolution in time given by

$$\mathcal{K}^t \varphi(\mathbf{x}) = \varphi(f^t(\mathbf{x})) = \exp(\lambda t)\varphi(\mathbf{x}), \tag{3.6}$$

where the observable function φ is called an eigenfunction of $\mathcal{K}^t$, and the associated number λ is the eigenvalue of $\mathcal{K}^t$.

Although the Koopman operator is linear, but one of its drawback is that this is infinite-dimensional. Consider the simple linear dynamical system in one dimension,

$$\dot{x} = \lambda x, \quad \lambda < 0. \tag{3.7}$$

The flow of (3.7) is given by $f^t(x) = \exp(\lambda t)x$. Let the observable function $\varphi(x) = x$, we

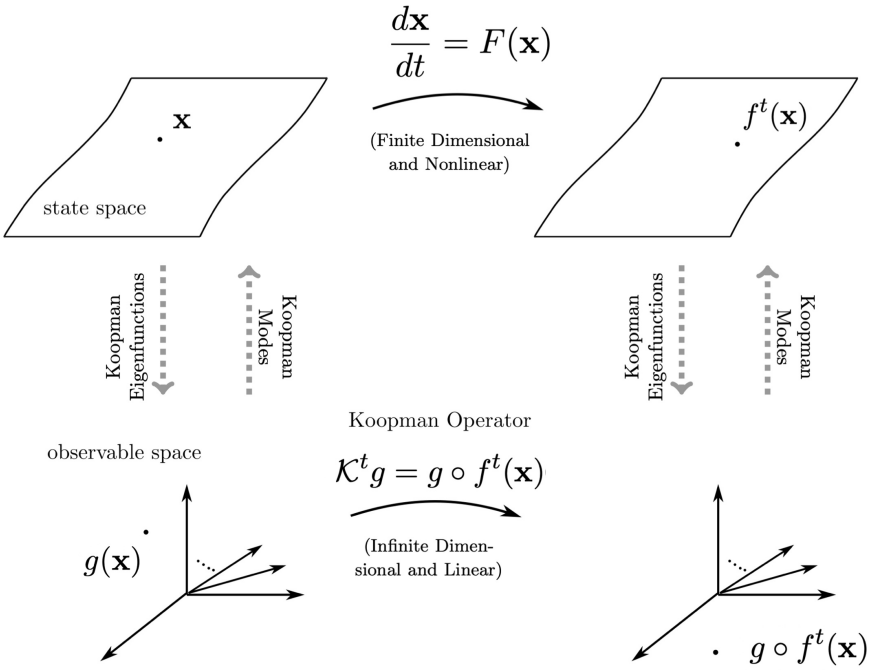

Figure 1: A figure of what is the impact of the Koopman operator and the relation to the dynamical system (the graph is modified based on the one from [2]). The top part evolves the state, $\mathbf{x} \in \mathcal{M}$, via the flow map $f^t(\mathbf{x})$. The bottom part evolves the observable, $g : \mathcal{M} \in \mathbb{C}$, via the Koopman operator, $\mathcal{K}^t$.

have

$$\mathcal{K}^t\varphi(x) = \varphi(x\exp(\lambda t)) = x\exp(\lambda t) = \exp(\lambda t)\varphi(x), \tag{3.8}$$

and $\varphi(x) = x$ is an eigenfunction of the Koopman operator corresponds with the eigenvalue λ. This is the result of the general property where the eigenvalues of the Koopman operator contain the system matrix spectrum for linear systems[21]. On the other hand, the eigen-pairs of the Koopman operator is more extensive than those of the "linear" operators, also it relies on the space of functions in which the evolution is occurring [7]. If we try the observable function $\varphi(x) = x^n, n \in \mathbb{Z}^+$, we have

$$\mathcal{K}^t\varphi(x) = \varphi(x\exp(\lambda t)) = x^n\exp(n\lambda t) = \exp(n\lambda t)\varphi(x). \tag{3.9}$$

That is, the functions $\varphi(x) = x^n$ are eigenfunctions of $\mathcal{K}^t$ associated with eigenvalues $n\lambda$. Although the dynamic system is linear and one-dimensional on the state space, the eigenfunctions of $\mathcal{K}^t$ can be much more complicated, and belongs to an infinite-dimensional vector space. These functions span the space of real-analytic functions on $\mathbb{R}$, thus we can use Koopman eigenfunctions to represent non-linear observables evolving under linear dynamics by a spectral expansion.

Corollary 1. A important property of the Koopman eigenfunction is that if φ_{λ_1} and λ_1 are the Koopman eigenfunction, then the product of two eigenfunctions is also an eigenfunction with eigenvalue $\lambda_1 + \lambda_2$. That is,

$$\begin{aligned}\mathcal{K}^t\left(\varphi_{\lambda_1}(\mathbf{x})\varphi_{\lambda_2}(\mathbf{x})\right) &= \varphi_{\lambda_1}\left(f^t(\mathbf{x})\right)\cdot\varphi_{\lambda_2}\left(f^t(\mathbf{x})\right)\\ &= \exp(\lambda_1 t)\,\varphi_{\lambda_1}(\mathbf{x})\exp(\lambda_2 t)\,\varphi_{\lambda_2}(\mathbf{x})\\ &= \exp\left((\lambda_1+\lambda_2)\,t\right)\varphi_{\lambda_1}(\mathbf{x})\varphi_{\lambda_2}(\mathbf{x}).\end{aligned} \tag{3.10}$$

Thus if λ is an eigenvalue with the corresponding eigenfunction φ_λ, then $n\lambda$ is also an eigenvalue for the associated eigenfunction ${\varphi_\lambda}^n$.

From the chain rule, we can derive the time derivative of the Koopman eigenfunction $\varphi(\mathbf{x})$ into

$$\frac{d}{dt}\varphi(\mathbf{x}) = [\nabla\varphi(\mathbf{x})] \cdot \dot{\mathbf{x}} = [\nabla\varphi(\mathbf{x})] \cdot F(\mathbf{x}). \tag{3.11}$$

We know that

$$\begin{aligned}\frac{d}{dt}\varphi(\mathbf{x}) = \lim_{\Delta t\to 0}\left[\frac{1}{\Delta t}(\mathcal{K}^t\varphi(\mathbf{x}) - \varphi(\mathbf{x}))\right] &= \lim_{\Delta t\to 0}\left[\frac{1}{\Delta t}(\varphi(f^{\Delta t}(\mathbf{x})) - \varphi(\mathbf{x}))\right] \\ &= \lim_{\Delta t\to 0}\left[\frac{e^{\lambda t}\varphi(\mathbf{x}) - \varphi(\mathbf{x})}{\Delta t}\right].\end{aligned} \tag{3.12}$$

Then by Taylor expansion we have

$$e^{\lambda t}\varphi(\mathbf{x}) = \varphi(\mathbf{x})(1 + \lambda\Delta t + \mathcal{O}(\Delta t^2)), \tag{3.13}$$

Since we know that Δt is small, so we can ignore $\mathcal{O}(\Delta t^2)$, and then the equation (3.12) becomes:

$$\lim_{\Delta t\to 0}\left[\frac{e^{\lambda t}\varphi(\mathbf{x}) - \varphi(\mathbf{x})}{\Delta t}\right] = \lim_{\Delta t\to 0}\left[\frac{\varphi(\mathbf{x})(1 + \lambda\Delta t) - \varphi(\mathbf{x})}{\Delta t}\right] = \lambda\varphi(\mathbf{x}). \tag{3.14}$$

Hence combined with equation (3.11)), we have the equivalent characterisation of the eigenfunctions $\varphi(\mathbf{x})$ as a PDE

$$\nabla\varphi(\mathbf{x}) \cdot F(\mathbf{x}) = \lambda\varphi(\mathbf{x}). \tag{3.15}$$

Given this linear PDE, it is possible to approximate the eigenfunctions by solving for the Laurent series, as in the few examples in [4]. This formulation assumes that the dynamics are both continuous and differentiable. In Section 3.3.4, we provide an example of determining the eigenvalues and eigenfunction in a given non-linear dynamical system by solving equation (3.15).

3.3 Koopman Mode Decomposition

We use $\mathbf{g}(\mathbf{x}) : \mathcal{M} \to \mathbb{R}^m$ to denote a vector-valued observable:

$$\mathbf{g}(\mathbf{x}) = \begin{bmatrix} g_1(\mathbf{x}) \\ g_2(\mathbf{x}) \\ \vdots \\ g_m(\mathbf{x}) \end{bmatrix}. \tag{3.16}$$

We can expand the individual observables in terms of the eigenfunctions $\varphi_{\lambda_j}(\mathbf{x})$, which provide a basis for Hilbert space:

$$g_i(\mathbf{x}) = \sum_{j=0}^{\infty} \hat{v}_{ij}\varphi_{\lambda_j}(\mathbf{x}) \tag{3.17}$$

Thus, the vector of observable $\mathbf{g}(\mathbf{x})$ can be expanded:

$$\mathbf{g}(\mathbf{x}) = \begin{bmatrix} g_1(\mathbf{x}) \\ g_2(\mathbf{x}) \\ \vdots \\ g_m(\mathbf{x}) \end{bmatrix} = \sum_{j=0}^{\infty} \varphi_{\lambda_j}(\mathbf{x})\hat{\mathbf{v}}_j \tag{3.18}$$

where $\hat{\mathbf{v}}_j$ is the j-th *Koopman mode* associated with the eigenfunction φ_{λ_j}

Definition 3.1 (Koopman mode [16])**.** The Koopman mode $\hat{\mathbf{v}}$ at an isolated eigenvalue λ of algebraic multiplicity 1 is the projection of $\mathbf{g}(\mathbf{x})$ onto the eigenfunction $\varphi_\lambda(\mathbf{x})$ of $\mathcal{K}^t$ at λ.

Hence we can define

$$\hat{\mathbf{v}}_j = \begin{bmatrix} \langle \varphi_{\lambda_j}, g_1 \rangle \\ \langle \varphi_{\lambda_j}, g_2 \rangle \\ \vdots \\ \langle \varphi_{\lambda_j}, g_m \rangle \end{bmatrix}, \tag{3.19}$$

where $\langle f, g \rangle = \int_{\mathcal{M}} f g dx$ is the inner product of functions in $\mathcal{M}$. When the observable is $\mathbf{g}(\mathbf{x}) = \mathbf{x}$, We would expect the Koopman modes to be coherent spatial modes with the same temporal dynamics that behave linearly. The Koopman modes $\hat{\mathbf{v}}$ are also known as DMD modes, and in Section 4 we discuss how to compute them.

Given the decomposition in (3.18), we can represent the dynamics of the observables of $\mathbf{g}$ as follows. In continues-time dynamical system,

$$\begin{aligned} \mathcal{K}^t(\mathbf{g}(\mathbf{x})) = \mathbf{g}\left(f^t(\mathbf{x_0})\right) &= \mathcal{K}^t\left(\sum_{j=0}^{\infty} \varphi_{\lambda_j}(\mathbf{x})\hat{\mathbf{v}}_j\right) \\ &= \sum_{j=0}^{\infty} \mathcal{K}^t \varphi_{\lambda_j}(\mathbf{x_0})\hat{\mathbf{v}}_j \\ &= \sum_{j=0}^{\infty} e^{\lambda_j t}\varphi_{\lambda_j}(\mathbf{x_0})\hat{\mathbf{v}}_j \end{aligned} \tag{3.20}$$

and in discrete-time dynamical system,

$$\mathcal{K}(\mathbf{g}(\mathbf{x})) = \sum_{j=0}^{\infty} \lambda_j \varphi_{\lambda_j}(\mathbf{x_0})\hat{\mathbf{v}}_j \tag{3.21}$$

This expansion is known as *Koopman Mode Decomposition(KMD)* of the observable $\mathbf{g}$ and was introduced by Mezić in 2005[15], and $\hat{\mathbf{v}}_j$ is the *Koopman mode* of $\mathbf{g}$ at the eigenvalue λ. Koopman modes are the vector-valued observable $\mathbf{g}$ projected onto the Koopman eigenfunctions. We can think $\hat{\mathbf{v}}_j$ as a structure within the data that evolves as $e^{\lambda_j t}$ over time. However this is only valid when the system $\dot{\mathbf{x}} = \mathbf{A}\mathbf{x}$ is linear. No one has demonstrated that such representations exist or are unique/convergent in general cases.

Now we can see that in Figure 1 there is a link between the two different operators acting on separate spaces as they capture the same dynamics, i.e., to compute $\mathcal{K}^t g(\mathbf{x})$ with state $\mathbf{x}$, we could either apply $\mathcal{K}$ on the observable g, followed by evaluation at $\mathbf{x}$ (the bottom section), or compute $f^t(\mathbf{x})$ and then evaluate g at the new position (the top section). Moreover, to compute $f^t(\mathbf{x})$, we could apply f^t to $\mathbf{x}$(the top section) or $\mathcal{K}$ to the full-state observable $g(\mathbf{x})$ and evaluate $(\mathcal{K}g)(\mathbf{x})$ (the bottom section). Then, we can choose to work with a finite-dimensional non-linear system or an infinite-dimensional linear system depending on which method is easier for the given problem.

3.3.1 Koopman Mode Decomposition in Linear System

Koopman modes are interesting because they resemble the eigenvector expansions utilised in linear dynamics.

Suppose the dynamical system $\dot{\mathbf{x}} = \mathbf{A}\mathbf{x}$ is linear, where $\mathbf{A} \in \mathbb{R}^{D\times D}$. Then the flow for

any initial state $\mathbf{x}_0$ is $\mathbf{x}(t) = e^{t\mathbf{A}}\mathbf{x}_0$. From equation (2.14) and equation (3.20), we have

$$\begin{aligned} f^t(\mathbf{x}) &= \sum_{j=1}^{D} a_j \mathbf{v}_j e^{\lambda_j t}, \quad \text{and} \\ \mathcal{K}^t(\mathbf{g}(\mathbf{x})) &= \sum_{j=1}^{\infty} e^{\lambda_j t} \varphi_{\lambda_j}(\mathbf{x}) \hat{\mathbf{v}}_j. \end{aligned} \tag{3.22}$$

Compare the coefficient of those time dependent terms in the above two equations we can get

$$a_j = \varphi_{\lambda_j}(\mathbf{x}), \quad \text{and} \quad \mathbf{v}_j = \hat{\mathbf{v}}_j. \tag{3.23}$$

On the other hand, we know that

$$\mathbf{A}\mathbf{v}_j = \lambda_j \mathbf{v}_j, \tag{3.24}$$

where λ_j and $\mathbf{v}_j$ are the eigenvalues and corresponding eigenvectors of $\mathbf{A}$. Now define an adjoint operator $*$ for the matrix $\mathbf{A}$ (or the transpose if $\mathbf{A}$ is real), so we have

$$\mathbf{A}^* \mathbf{w}_j = \lambda_j^* \mathbf{w}_j, \tag{3.25}$$

where λ_j^* is the complex conjugate of λ_j and $\mathbf{w}_j$ is the *left* eigenvectors of $\mathbf{A}$.

Now we look at the quantity $\mathbf{v}_j$ and $\mathbf{w}_j$

$$\langle \mathbf{A}\mathbf{v}_i, \mathbf{w}_j \rangle, \tag{3.26}$$

where $\langle \mathbf{x}, \mathbf{y} \rangle = \mathbf{x} \cdot \mathbf{y}$ denotes the inner product on $\mathbb{R}^D$. By the definition of inner product, we have

$$\langle \mathbf{A}\mathbf{v}_i, \mathbf{w}_j \rangle = \langle \mathbf{v}_i, \mathbf{A}^* \mathbf{w}_j \rangle, \tag{3.27}$$

and by equation(3.24) and equation(3.25), we have

$$\begin{aligned} \langle \mathbf{A}\mathbf{v}_i, \mathbf{w}_j \rangle &= \langle \lambda_i \mathbf{v}_i, \mathbf{w}_j \rangle = \lambda_i \langle \mathbf{v}_i, \mathbf{w}_j \rangle, \\ \langle \mathbf{v}_i, \mathbf{A}^* \mathbf{w}_j \rangle &= \langle \mathbf{v}_i, \lambda_j^* \mathbf{w}_j \rangle = \lambda_j \langle \mathbf{v}_i, \mathbf{w}_j \rangle. \end{aligned} \tag{3.28}$$

Therefore, it follows that

$$(\lambda_i - \lambda_j) \langle \mathbf{v}_i, \mathbf{w}_j \rangle = 0. \tag{3.29}$$

Hence if $\lambda_i \neq \lambda_j$, then $\langle \mathbf{v}_i, \mathbf{w}_j \rangle = 0$, which implies that $\mathbf{v}_i, \mathbf{w}_j$ are biorthogonal, so that the two basis $\{\mathbf{v}_j\}$ and $\{\mathbf{w}_j\}$ can be normalised according to the condition $\langle \mathbf{v}_i, \mathbf{w}_j \rangle = \delta_{ij}$. From equation (2.13) we have

$$\mathbf{x} = \sum_{j=1}^{D} a_j \mathbf{v}_j, \tag{3.30}$$

therefore

$$\langle \mathbf{x}, \mathbf{w}_i \rangle = \sum_{j=1}^{D} a_j \mathbf{v}_j \mathbf{w}_i = \sum_{j=1}^{D} a_j \delta_{ij} = a_i = \varphi_{\lambda_j}(\mathbf{x}). \tag{3.31}$$

Hence we showed that

$$\varphi_{\lambda_j}(\mathbf{x}) = \langle \mathbf{x}, \mathbf{w}_i \rangle. \tag{3.32}$$

So the eigenfunction is the projection of the state onto the left eigenvector. And if equation

(3.32) is true, then it is true that

$$\mathbf{x} = \sum_{j=1}^{D} \varphi_{\lambda_j} \hat{\mathbf{v}}_j, \tag{3.33}$$

Since the Koopman modes coincide with the eigenvectors of A if this is a linear system with the specific choice of observable $\mathbf{g}(\mathbf{x}) = \mathbf{x}$.

3.3.2 Koopman Mode Decomposition in Non-linear System

Consider a non-linear system $\dot{\mathbf{x}} = \mathbf{F}(\mathbf{x})$ with a hyperbolic fixed point. Then Theorem 2.1 tells us that, locally, the linearised flow we find near the fixed point approximate the full non-linear problem. Which means that there is an invertible coordinate transformation $\mathbf{y} = h(\mathbf{x})$ such that $\dot{\mathbf{y}} = \mathbf{A}\mathbf{y}$ is a linear system with the solution $\mathbf{y}(t) = e^{t\mathbf{A}}\mathbf{y}(0)$ and such that

$$f^t(\mathbf{x}) = h^{-1}\left(e^{t\mathbf{A}} h(\mathbf{x})\right). \tag{3.34}$$

So we can solve the non-linear system by transforming it to the state space $\mathbf{y}$, then solving the linear system and transforming it back to the state space $\mathbf{x}$. We demonstrate the Koopman linear expansion for linear systems first, and then derive the expansion for non-linear systems by the topological conjugate.

Let $\{\mathbf{v}_j\}_{j=1}^{D}$ and $\{\lambda_j\}_{j=1}^{D}$ denote the eigen-pairs of $\mathbf{A}$. From equation 3.32, the Koopman eigenfunctions are

$$\tilde{\varphi}_{\lambda_j}(\mathbf{y}) = < \mathbf{y}, \mathbf{w}_j >, \tag{3.35}$$

where $\mathbf{w}_j$ is the normalised eigenvector of $\mathbf{A}^*$. It is straightforward to demonstrate that the eigenfunctions of the Koopman operator for the non-linear system are $\varphi_{\lambda_j}(\mathbf{x}) = \tilde{\varphi}_{\lambda_j}(h(\mathbf{x}))$. We can use Corollary 1 to construct other Koopman eigenfunctions. We can derive the Koopman expansion for the non-linear system by transform $\mathbf{y}$ into a decoupled linear system $\mathbf{y} = \mathbf{E}\mathbf{z}$. If the matrix A is diagonalisable and E is the matrix whose columns are eigenvectors of $\mathbf{A}$, then the Koopman eigenfunctions are equivalent to the state variables of the diagonal system, i.e.,

$$\begin{aligned} \mathbf{z} &= [\mathbf{z}_{\lambda_1}, \mathbf{z}_{\lambda_2}, \ldots, \mathbf{z}_{\lambda_D}]^T = \mathbf{E}^{-1}\mathbf{y} = [\tilde{\varphi}_{\lambda_1}(\mathbf{y}), \tilde{\varphi}_{\lambda_2}(\mathbf{y}), \ldots, \tilde{\varphi}_{\lambda_D}(\mathbf{y})]^T \\ &= [\varphi_{\lambda_1}(\mathbf{x}), \varphi_{\lambda_2}(\mathbf{x}), \ldots, \varphi_{\lambda_D}(\mathbf{x})]^T. \end{aligned} \tag{3.36}$$

Now consider the vector observable of the non-linear dynamical system $\mathbf{g}(\mathbf{x}) = \mathbf{g}\left(h^{-1}(\mathbf{y})\right) = \mathbf{g}\left(h^{-1}(\mathbf{E}\mathbf{z})\right) = \tilde{\mathbf{g}}(\mathbf{z})$ where $\tilde{\mathbf{g}}$ is real analytic in $\mathbf{z}$. Hence we have

$$\begin{aligned} \mathbf{g}(\mathbf{x}) = \tilde{\mathbf{g}}(\mathbf{z}) &= \sum_{j=1}^{D} \mathbf{z}_{\lambda_j} \hat{\mathbf{v}}_j, \\ &= \sum_{j=1}^{D} \varphi_{\lambda_j} \hat{\mathbf{v}}_j, \end{aligned} \tag{3.37}$$

Using Corollary 1, we can write the Koopman linear expansion of $\mathbf{g}$ as

$$\mathcal{K}^t \mathbf{g} = \sum_{j=1}^{D} e^{\lambda_j t} \varphi_{\lambda_j} \hat{\mathbf{v}}_j \tag{3.38}$$

We know that Theorem 2.1 tells us that, locally, a conjugacy exists for a small neighbourhood of the fixed point for non-linear systems. However, by using properties of the

Koopman eigenfunctions, the results in [17] have extended the conjugacy to the entire basin of attraction for stable fixed points.

3.3.3 Detailed Analysis of a Simple Non-linear System

We use the same example as in [4] for a detailed Koopman analysis. In that reference, it was shown that one can augment the state x (the first component of $\mathbf{x} = (x, y)^T$) with the non-linear observable $g = x^2$, to define a three-dimensional Koopman invariant subspace, and discussed the effect of incorrect observables to the Koopman eigenvalues. However, here we show another way of solving this non-linear system via a near-identity transformation that provides the eigenfunction of the system, and we also try out different observables into this system and determine its eigenfunction and test the error between the observable and the Koopman mode decomposition. Finally we explore the connections between the Koopman eigenfunctions and invariant of the linearised system,

Example 3.1. Consider a non-linear planar dynamical system

$$\begin{aligned} \dot{x} &= \mu x, \\ \dot{y} &= \lambda \left(y - x^2 \right), \end{aligned} \tag{3.39}$$

where $\lambda, \mu < 0$. We can see that there is only one fixed point in this system, which is the origin, and the eigenvalues of the system linearised system around the origin are μ and λ respectively. Hence this equilibrium is stable. Furthermore, the system has invariant manifolds given by $x = 0$ and $y = -\frac{\lambda x^2}{2\mu - \lambda}$ as shown in Figure 2a: If the states lies on one of these curves at some time t, it will remain on it for all time. And Figure 2b shows the phase portrait of the system that we can see it towards to origin as the time goes on. By

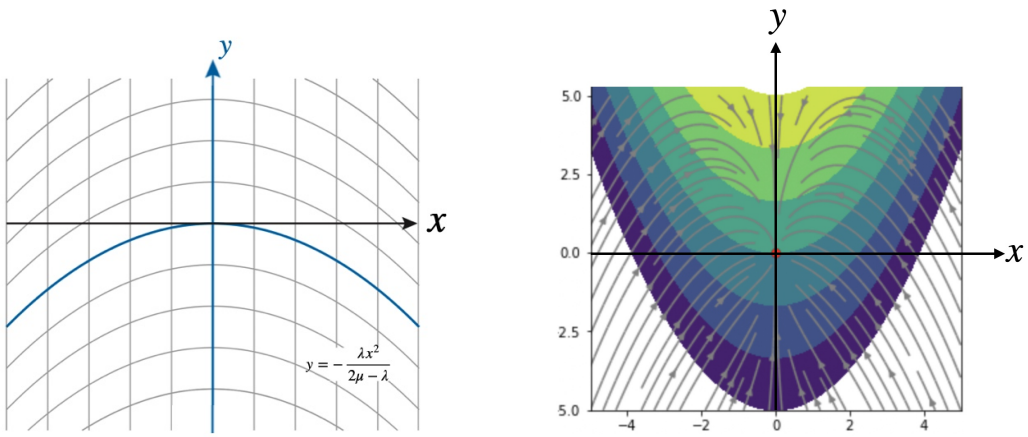

(a) Phase plane

(b) Phase portrait

Figure 2: (a) Phase plane for System 3.39 with $\mu = -0.1$ and $\lambda = -0.5$. The grey lines denote the level sets of the Koopman eigenfunctions $\varphi_\mu(vertical)$ and $\varphi_\lambda(curved)$. The invariant manifolds are represented by the thick lines. (b) Phase portrait with contour plot for System 3.39 with $\mu = -0.1$ and $\lambda = -0.5$.. The red dot in the centre denote the origin, and the grey lines with arrow represent the flow of the system, and the colour is the different levels sets.

equation(2.4) we can derive the flow of the system(3.7) which is

$$f^t(\mathbf{x}) = \begin{bmatrix} xe^{\mu t} \\ (y + \frac{\lambda x^2}{2\mu - \lambda})e^{\lambda t} - \frac{\lambda x^2}{2\mu - \lambda} e^{2\mu t} \end{bmatrix}. \tag{3.40}$$

Now applying near-identity transforms on system(3.39). We write the dynamical sys-

tem in the form:

$$\dot{\mathbf{x}} = \mathbf{\Lambda x} + \mathbf{F}_2(\mathbf{x}) + \cdots, \tag{3.41}$$

and define the transform

$$\mathbf{x} = \boldsymbol{\xi} + \mathbf{h}_2(\boldsymbol{\xi}), \quad \text{where } \mathbf{h}_2(\boldsymbol{\xi}) = \begin{pmatrix} a_{20}\xi^2 + a_{11}\xi\eta + a_{02}\eta^2 \\ b_{20}\xi^2 + b_{11}\xi\eta + b_{02}\eta^2 \end{pmatrix}. \tag{3.42}$$

with the inverse

$$\boldsymbol{\xi} = \mathbf{x} - \mathbf{h}_2(\mathbf{x}) + \mathcal{O}\left(|\mathbf{x}|^3\right). \tag{3.43}$$

Then differentiating the transform with respect to time gives

$$\dot{\mathbf{x}} = (\mathbf{I} + D\mathbf{h}_2)\,\dot{\boldsymbol{\xi}}, \tag{3.44}$$

so we can write the original system in $\boldsymbol{\xi}$ with equation(3.42)

$$(\mathbf{I} + D\mathbf{h}_2)\,\dot{\boldsymbol{\xi}} = \mathbf{\Lambda}\boldsymbol{\xi} + \mathbf{\Lambda}\mathbf{h}_2(\boldsymbol{\xi}) + \mathbf{F}_2(\boldsymbol{\xi}) + \mathcal{O}\left(|\boldsymbol{\xi}|^3\right). \tag{3.45}$$

By Taylor expansion we have

$$(\mathbf{I} + D\mathbf{h}_2)^{-1} = \mathbf{I} - D\mathbf{h}_2 + \mathcal{O}\left(|\boldsymbol{\xi}|^3\right), \tag{3.46}$$

so the dynamics of $\boldsymbol{\xi}$ is governed by

$$\dot{\boldsymbol{\xi}} = \mathbf{\Lambda}\boldsymbol{\xi} - D\mathbf{h}_2\mathbf{\Lambda}\boldsymbol{\xi} + \mathbf{\Lambda}\mathbf{h}_2(\boldsymbol{\xi}) + \mathbf{F}_2(\boldsymbol{\xi}) + \mathcal{O}\left(|\boldsymbol{\xi}|^3\right). \tag{3.47}$$

Therefore, we need to impose the following condition

$$0 = f_2(\boldsymbol{\xi}) - D\mathbf{h}_2\mathbf{\Lambda}\boldsymbol{\xi} + \mathbf{\Lambda}\mathbf{h}_2(\boldsymbol{\xi}). \tag{3.48}$$

Hence from the explicit transform (3.42) for $\boldsymbol{\xi}$, we find the Jacobian of $\mathbf{h}_2(\boldsymbol{\xi})$ is

$$D\mathbf{h}_2(\boldsymbol{\xi}) = \begin{pmatrix} 2a_{20}\xi + a_{11}\eta & 2a_{02}\eta + a_{11}\xi \\ 2b_{20}\xi + b_{11}\eta & 2b_{02}\eta + b_{11}\xi \end{pmatrix}. \tag{3.49}$$

And by comparing the coefficient of $\boldsymbol{\xi}$ in equation (3.48), we have the following result

$$b_{20} = -\frac{\lambda}{2\mu - \lambda}, \quad \text{everywhere else is zero.} \tag{3.50}$$

Substituting this result back into equation(3.42), we can see the transformed linear dynamical system is

$$\begin{matrix} \dot{\xi} = \mu\xi \\ \dot{\eta} = \lambda\eta \end{matrix} \quad \text{with} \quad \begin{matrix} \xi = x \\ \eta = y + \dfrac{\lambda x^2}{2\mu - \lambda}. \end{matrix} \tag{3.51}$$

The Koopman eigenfunctions of equation(3.40) corresponding to eigenvalues μ and λ are

$$\varphi_\mu = x \quad \text{and} \quad \varphi_\lambda = y + \frac{\lambda x^2}{2\mu - \lambda}. \tag{3.52}$$

To verify these Koopman eigenfunctions, we can use the flow map (3.40) to get

$$\begin{aligned} \mathcal{K}^t\varphi_\mu(x) &= \varphi_\mu(f^t(\mathbf{x})) = xe^{\mu t} \\ \mathcal{K}^t\varphi_\lambda(x) &= \varphi_\lambda(f^t(\mathbf{x})) = \left(y + \frac{\lambda x^2}{2\mu - \lambda}\right)e^{\lambda t}, \end{aligned} \tag{3.53}$$

exactly the definition as in the system (3.39).

Now suppose our observable function is $\mathbf{g}(\mathbf{x}) = \mathbf{x}$, then by equation(3.20), we have

$$\mathcal{K}^t(\mathbf{g}(\mathbf{x})) = f^t(\mathbf{x}) = \begin{bmatrix} xe^{\mu t} \\ \left(y + \frac{\lambda x^2}{2\mu - \lambda}\right) e^{\lambda t} - \frac{\lambda x^2}{2\mu - \lambda} e^{2\mu t} \end{bmatrix} = \left(y + \frac{\lambda x^2}{2\mu - \lambda}\right) e^{\lambda t}\hat{\mathbf{x_1}} + xe^{\mu t}\hat{\mathbf{x_2}} + x^2 e^{2\mu t}\hat{\mathbf{x_3}} \tag{3.54}$$

Hence we have the result for the Koopman mode for $\mathbf{g}(\mathbf{x}) = \mathbf{x}$ with eigenvalues $\lambda, \mu, 2\mu$ respectively

$$\hat{\mathbf{x_1}} = \begin{pmatrix} 0 \\ 1 \end{pmatrix} \quad \hat{\mathbf{x_2}} = \begin{pmatrix} 1 \\ 0 \end{pmatrix} \quad \hat{\mathbf{x_3}} = \begin{pmatrix} 0 \\ -\frac{\lambda}{2\mu - \lambda} \end{pmatrix}. \tag{3.55}$$

Hence we have our Koopman mode decomposition with observable function $\mathbf{g}(\mathbf{x}) = \mathbf{x}$

$$\mathcal{K}^t(\mathbf{g}(\mathbf{x})) = \left(y + \frac{\lambda x^2}{2\mu - \lambda}\right) e^{\lambda t} \begin{pmatrix} 0 \\ 1 \end{pmatrix} + xe^{\mu t} \begin{pmatrix} 1 \\ 0 \end{pmatrix} + x^2 e^{2\mu t} \begin{pmatrix} 0 \\ -\frac{\lambda}{2\mu - \lambda} \end{pmatrix}. \tag{3.56}$$

In Figure 3a (the left one), we take the initial point $(1, 1)^T$ and plot the exact flow against the flow computed by KMD with $t = 60$. We can see that they are almost identical, and in fact for the figure on the right, we also plotted the error between the exact flow and the KMD flow. We can see that the error is basically 0 for all time t. This is a special case of KMD where we only used 3 terms to represent the non-linear system with the observable function $\mathbf{g}(\mathbf{x}) = \mathbf{x}$.

Alternatively, if we let the observable function be $\mathbf{g}(\mathbf{x}) = e^{\mathbf{x}}$, then

$$\mathcal{K}^t(\mathbf{g}(\mathbf{x})) = \exp(f^t(\mathbf{x})) = \begin{bmatrix} \exp\left(xe^{\mu t}\right) \\ \exp\left(\left(y + \frac{\lambda x^2}{2\mu - \lambda}\right) e^{\lambda t} - \frac{\lambda x^2}{2\mu - \lambda} e^{2\mu t}\right) \end{bmatrix}. \tag{3.57}$$

So by Taylor expansion, we can write

$$\exp\left(xe^{\mu t}\right) = \sum_{n=0}^{\infty} \frac{x^n e^{n\mu x}}{n!} = 1 + xe^{\mu x} + \frac{x^2 e^{2\mu x}}{2} + \cdots \tag{3.58}$$

and here shows that we have eigenvalue with $0, \mu, 2\mu, 3\mu, ...\infty$ with corresponding eigenfunction $\varphi_\mu^0 \equiv 1, \varphi_\mu, \varphi_\mu^2, \varphi_\mu^3, ..., \varphi_\mu^\infty$ in the top equation of (3.58). Hence the Koopman mode can be written as

$$\hat{\mathbf{x_1}} = \begin{pmatrix} 1 \\ 0 \end{pmatrix} \quad \hat{\mathbf{x_2}} = \begin{pmatrix} 1 \\ 0 \end{pmatrix} \quad \hat{\mathbf{x_3}} = \begin{pmatrix} \frac{1}{2} \\ 0 \end{pmatrix} \quad ... \quad \hat{\mathbf{x_n}} = \begin{pmatrix} \frac{1}{n!} \\ 0 \end{pmatrix}, \cdots. \tag{3.59}$$

Now using Taylor expansion in the bottom equation of (3.58), we have

$$\begin{aligned} &\exp\left(\left(y + \frac{\lambda x^2}{2\mu - \lambda}\right) e^{\lambda t} - \frac{\lambda x^2}{2\mu - \lambda} e^{2\mu t}\right) = \sum_{n=0}^{\infty} \frac{((y + \frac{\lambda x^2}{2\mu - \lambda})e^{\lambda t} - \frac{\lambda x^2}{2\mu - \lambda} e^{2\mu t})^n}{n!} \\ &= 1 + \left(\left(y + \frac{\lambda x^2}{2\mu - \lambda}\right) e^{\lambda t} - \frac{\lambda x^2}{2\mu - \lambda} e^{2\mu t}\right) + \frac{((y + \frac{\lambda x^2}{2\mu - \lambda})e^{\lambda t} - \frac{\lambda x^2}{2\mu - \lambda} e^{2\mu t})^2}{2} + ..., \end{aligned} \tag{3.60}$$

we can see that if we expand the third term, this gives eigenvalue with $(2\mu + \lambda), 2\lambda$ and 4μ with corresponding eigenfunctions $\varphi_\lambda, \varphi_\mu^2, \varphi_\lambda^2$ and φ_μ^4, with more terms expanded when

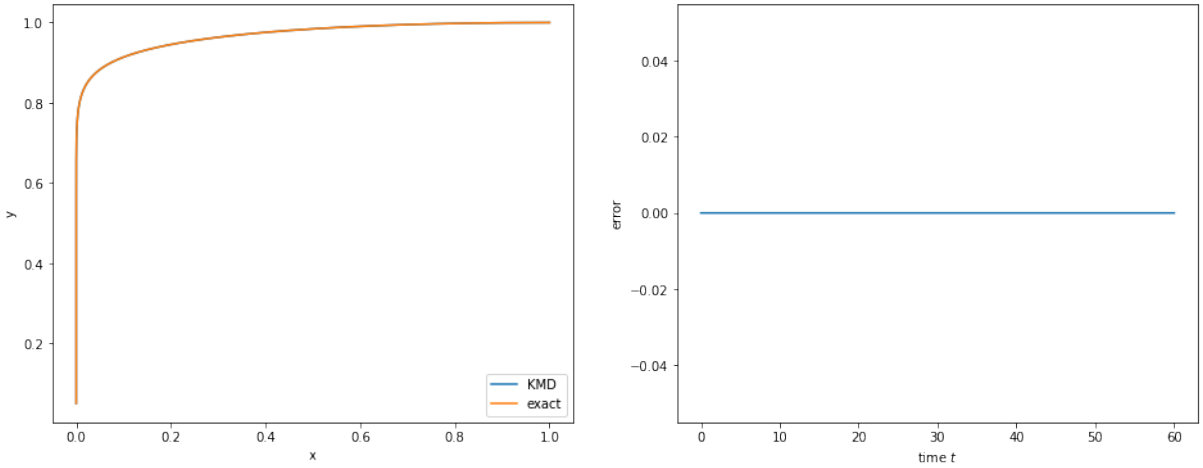

(a) Observable function $\mathbf{g}(\mathbf{x}) = \mathbf{x}$

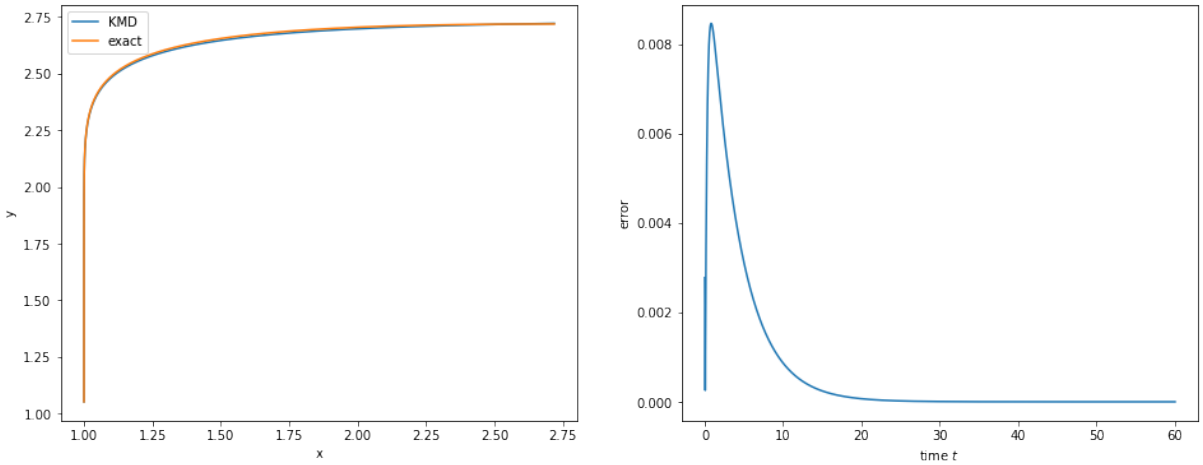

(b) Observable function $\mathbf{g}(\mathbf{x}) = e^{\mathbf{x}}$

Figure 3: The flow of the observable function against the flow computed by Koopman mode decomposition and the error between the exact flow and the Koopman mode decomposition with the initial point $(1, 1)$ and time $t = 60$ for the non-linear system (3.39).

carrying on. Hence we can write the Koopman mode as

$$\hat{\mathbf{x_1}} = \begin{pmatrix}0\\1\end{pmatrix}, \quad \hat{\mathbf{x_2}} = \begin{pmatrix}0\\1\end{pmatrix}, \quad \hat{\mathbf{x_3}} = \begin{pmatrix}0\\-\frac{\lambda}{2\mu-\lambda}\end{pmatrix}, \quad \hat{\mathbf{x_4}} = \begin{pmatrix}0\\-\frac{\lambda}{2\mu-\lambda}\end{pmatrix},$$
$$\hat{\mathbf{x_5}} = \begin{pmatrix}0\\\frac{1}{2}\end{pmatrix}, \quad \hat{\mathbf{x_6}} = \begin{pmatrix}0\\\frac{\lambda}{2(2\mu-\lambda)}\end{pmatrix}, \quad \cdots . \tag{3.61}$$

Combining equation(3.59) and equation(3.61), we have the full list of eigenfunction and eigenvalues, so we can write Koopman mode decomposition with the observable function $\mathbf{g}(\mathbf{x}) = e^{\mathbf{x}}$, i.e.,

$$\begin{aligned}\mathcal{K}^t(\mathbf{g}(\mathbf{x})) = {} & 1e^{0t}\begin{pmatrix}1\\0\end{pmatrix} + xe^{\mu t}\begin{pmatrix}1\\0\end{pmatrix} + x^2e^{2\mu t}\begin{pmatrix}\frac{1}{2}\\0\end{pmatrix} + x^3e^{3\mu t}\begin{pmatrix}\frac{1}{6}\\0\end{pmatrix} + ... \\ & + 1e^{0t}\begin{pmatrix}0\\1\end{pmatrix} + \left(y + \frac{\lambda x^2}{2\mu-\lambda}\right)e^{\lambda t}\begin{pmatrix}0\\1\end{pmatrix} + x^2e^{2\mu t}\begin{pmatrix}0\\-\frac{\lambda}{2\mu-\lambda}\end{pmatrix} \\ & + x^2\left(y + \frac{\lambda x^2}{2\mu-\lambda}\right)e^{(2\mu+\lambda)t}\begin{pmatrix}0\\-\frac{\lambda}{2\mu-\lambda}\end{pmatrix} + \left(y + \frac{\lambda x^2}{2\mu-\lambda}\right)^2 e^{2\lambda t}\begin{pmatrix}0\\\frac{1}{2}\end{pmatrix} + x^4e^{4\mu t}\begin{pmatrix}0\\\frac{\lambda}{2(2\mu-\lambda)}\end{pmatrix} \\ & + ...\end{aligned} \tag{3.62}$$

which is made by infinite terms of different combination of φ_μ and φ_λ.

In Figure 3b, we use the first five terms from the Taylor expansion to simulate the flow of the observable function $\mathbf{g}(\mathbf{x}) = e^{\mathbf{x}}$; we can see that the difference between the exact flow and KMD flow is still small and tends to 0 as time goes on. In the right figure, we can see that the error goes up very quickly temperorily and then decreases exponentially to zero after that; this happens the flow changes its direct. Because we only use a finite number of terms in the Taylor expansion to simulate the flow of the observables, a slight error between the exact flow and the KMD flow seems reasonable. If we increase the number of Taylor expansion terms, we can reduce the error between them. Ideally, suppose we use infinite many Taylor expansion terms of the modes with the corresponding eigenvalues and eigenfunctions to simulate the observable $\mathbf{g}(\mathbf{x})$. In that case, we can match the two flows even closer. Hence we show that we could use the Koopman operator to represent a non-linear system into infinitely many combinations of the finite linear systems.

Now if we look the linearlised system(3.51), we can see that the eigenfunction of the system has been changed to $\xi e^{\mu t}$ and $\eta e^{\lambda t}$, so the Koopman mode decomposition with the observable function $\mathbf{g}(\boldsymbol{\xi}) = \boldsymbol{\xi} = (\xi, \eta)^T$ becomes

$$\mathcal{K}^t(\mathbf{g}(\boldsymbol{\xi})) = \xi e^{\mu t}\begin{pmatrix}1\\0\end{pmatrix} + \eta e^{\lambda t}\begin{pmatrix}0\\1\end{pmatrix} = xe^{\mu t}\begin{pmatrix}1\\0\end{pmatrix} + \left(y + \frac{\lambda x^2}{2\mu-\lambda}\right)e^{\lambda t}\begin{pmatrix}0\\1\end{pmatrix}. \tag{3.63}$$

Hence we can see that from the near-identity transform, we have the basis eigenvalues and eigenfunctions from the equation(3.51). Let us bring it back to the non-linear system(3.39). We can span those eigenvalues into the simple invariant solution and eigenfunctions as the Koopman invariant subspace to get the Koopman mode decomposition with any observable function $\mathbf{g}(\mathbf{x})$. Therefore if we have a non-linear system, we can first transform it into a linear system and determine its eigenvalues and eigenfunctions. We can span them to find the eigenvalues and eigenfunctions of the non-linear system. However, this result only works in the system with a single isolated fixed point.

3.3.4 Determine Eigen-pairs by Solving the governing PDE

Here we introduce an alternative way to determine the eigenvalues and eigenfunctions for Example 3.1 discussed above. From the characterising equation (3.15) for Koopman eigenvalue s and eigenfunction φ_s, we have the PDE

$$[\nabla\varphi_s(\mathbf{x})] \cdot F(\mathbf{x}) = s\varphi_s(\mathbf{x}), \tag{3.64}$$

or more specifically,

$$\mu x\frac{\partial\varphi_s}{\partial x} + \lambda(y - x^2)\frac{\partial\varphi_s}{\partial y} = s\varphi_s(\mathbf{x}). \tag{3.65}$$

By the method of characteristics, we first solve the following systems

$$\frac{dx}{d\tau} = \mu x, \quad \frac{dy}{d\tau} = \lambda(y - x^2), \quad \frac{d\varphi_s}{d\tau} = s\varphi_s. \tag{3.66}$$

The first and the third equation can be solved directly, i.e.,

$$x(\tau) = \exp(\mu\tau)x(0) = e^{\mu\tau}x_0, \qquad \varphi_s(s) = e^{s\tau}\varphi_s(0).$$

Substituting the solution $x(t)$ into the second equation in the system (3.66), y can be solved as

$$y = \left(y_0 + \frac{\lambda x_0^2}{2\mu - \lambda}\right)e^{\lambda t} - \frac{\lambda x_0^2}{2\mu - \lambda}e^{2\mu t}.$$

To get the solution for the PDE (3.65), we have to eliminate the variable τ in the solutions for $x(\tau), y(\tau)$ and $\varphi_s(\tau)$. That is,

$$\frac{1}{\mu}\ln x - \frac{1}{s}\ln\varphi_s = \frac{1}{\mu}\ln x_0 - \frac{1}{s}\ln\varphi_s(0) = c_1 \tag{3.67}$$

for some constant c_1, and

$$\begin{aligned} y = (y_0 + \frac{\lambda x_0^2}{2\mu - \lambda})e^{\lambda\tau} - \frac{\lambda x_0^2}{2\mu - \lambda}e^{2\mu\tau} &= (y_0 + \frac{\lambda x_0^2}{2\mu - \lambda})(\frac{x}{x_0})^{\frac{\lambda}{\mu}} - \frac{\lambda x_0^2}{2\mu - \lambda}\frac{x^2}{x_0^2} \\ &= (y_0 + \frac{\lambda x_0^2}{2\mu - \lambda})(\frac{x}{x_0})^{\frac{\lambda}{\mu}} - \frac{\lambda x^2}{2\mu - \lambda}. \end{aligned} \tag{3.68}$$

The last equation implies that

$$\frac{y + \frac{\lambda x^2}{2\mu - \lambda}}{x^{\frac{\lambda}{\mu}}} = \frac{y_0 + \frac{\lambda x_0^2}{2\mu - \lambda}}{x_0^{\frac{\lambda}{\mu}}} = c_2. \tag{3.69}$$

Therefore, the general solution of the equation for the eigenfunction φ_s can be obtained from the previous two equations (3.67) and (3.69). That is,

$$\frac{1}{\mu}\ln x - \frac{1}{s}\ln\varphi_s = G\left(\frac{y + \frac{\lambda x^2}{2\mu - \lambda}}{x^{\frac{\lambda}{\mu}}}\right), \tag{3.70}$$

where G is an arbitrary function. In other words, the eigenfunction φ_s becomes

$$\varphi_s = x^{\frac{s}{\mu}}\exp\left(s \cdot G\left(\frac{y + \frac{\lambda x^2}{2\mu - \lambda}}{x^{\frac{\lambda}{\mu}}}\right)\right). \tag{3.71}$$

So the Koopman mode decomposition can be written as

$$\mathcal{K}^t\mathbf{g}(\mathbf{x}) = \sum_n^{\infty} x^{\frac{\lambda_n}{\mu}} \exp\left(s \cdot G\left(\frac{y + \frac{\lambda x^2}{2\mu - \lambda}}{x^{\frac{\lambda}{\mu}}}\right)\right) e^{\lambda_n t}\hat{\mathbf{x}_\mathbf{n}}, \tag{3.72}$$

with an arbitrary function G.

The two methods above of exploring Koopman mode decomposition in a non-linear system are equivalent. The first method is transforming a non-linear system into a linear system and determining its eigenvalues and eigenfunctions. We find that any finite collection of the eigenfunctions forms a Koopman invariant subspace, and we can obtain that the Koopman invariant subspace includes the original state variables. If we make a special choice of the observable functions, as we did in the Example 3.1 with the observable functions $\mathbf{g}(\mathbf{x}) = (x, y, x^2)$, then we get a finite-dimensional linear system to evolve these observables forward in time. The advantage of this method is that we can derive the full Koopman mode decomposition easily. However, this method is limited that we can only use a single isolated fixed point system. Because for the system has multiple fixed points, it is not globally topologically conjugate to a finite-dimensional linear system, hence it cannot be represented by a finite-dimensional linear Koopman subspace that contains all possible states [3]. The second method is solving PDEs using standard techniques, and we can derive the Koopman eigenfunction by solving an even more complicated PDE.

In practice, we would have more complex non-linear systems, so we need employ numerical methods to solve them. Typically, we can approximate the Koopman mode decomposition as a truncated sum of a few dominant terms like we did above in Example 3.1. The Koopman mode decomposition is connected to data-driven modelling via Dynamic mode decomposition(DMD)[21]. The DMD eigenvalues and DMD modes will approximate the Koopman eigenvalues and Koopman modes, and the amplitude of the DMD mode will approximate the corresponding Koopman eigenfunction evaluated at the initial condition $\varphi_{\lambda_j}(x_0)$.

4 Numerical Methods for Koopman Mode Analysis

Acquisition of linear representations for non-linear systems has the potential to revolutionise our ability to predict these systems. Theorem 2.1 tells us that the linearisation of dynamical systems near the fixed point can be employed for local linear representations of the dynamics. However, it is difficult to obtain finite-dimensional approximations of the Koopman operator introduced in the previous chapter. In [16], Mezić introduces a theoretical algorithm known as Generalised Laplace Analysis that can be used to compute Koopman mode decomposition.

Theorem 4.1 (Generalised Laplace Analysis [16])**.** Let $\lambda_1, ..., \lambda_K$ be the eigenvalues of the Koopman operator $\mathcal{K}^t$ such that $|\exp(\lambda_0)| \geq |\exp(\lambda_1)| \geq \cdots \geq |\exp(\lambda_K)|$. Then the Koopman mode associated with λ_K is obtained by computing

$$\varphi_K(\mathbf{x})\hat{\mathbf{v}}_K = \lim_{T\to\infty} \frac{1}{T} \int_0^T e^{-\lambda_K t} \left[\mathbf{g}\left(f^t(\mathbf{x})\right) - \sum_{j=0}^{K-1} e^{\lambda_j t} \varphi_j(\mathbf{x})\hat{\mathbf{v}}_j \right] dt. \tag{4.1}$$

Proof. We have

$$\mathbf{g}\left(f^t(\mathbf{x})\right) = \sum_{j=0}^{\infty} e^{\lambda_j t} \varphi_{\lambda_j}(\mathbf{x})\hat{\mathbf{v}}_j. \tag{4.2}$$

Let $t \to \infty$, and from the condition $|\exp(\lambda_0)| \geq |\exp(\lambda_1)| \geq \cdots \geq |\exp(\lambda_K)|$, we can observe that

$$\mathbf{g}\left(f^t(\mathbf{x})\right) \sim e^{\lambda_0 t} \varphi_0 \mathbf{x}\hat{\mathbf{v}}_0. \tag{4.3}$$

When $t \to \infty$, the above exponential term grows much faster than any other terms, so $e^{\lambda_0 t}$ is the dominating term in this series.
Now we can claim that

$$\lim_{t\to\infty} e^{-\lambda_0 t} \cdot \mathbf{g}\left(f^t(\mathbf{x})\right) = \varphi_0(\mathbf{x})\,\hat{\mathbf{v}}_0, \tag{4.4}$$

Use induction on the number of terms taken in the summation, we can assume that

$$\mathbf{g}\left(f^t(\mathbf{x})\right) - \sum_{j=0}^{K-1} e^{\lambda_j t} \varphi_j(\mathbf{x})\hat{\mathbf{v}}_j = \sum_{j=K}^{\infty} e^{\lambda_j t} \varphi_j(\mathbf{x})\hat{\mathbf{v}}_j. \tag{4.5}$$

As $t \to \infty$, the dominating term on the right hand side will be $e^{\lambda_K t}\varphi_K(\mathbf{x})\hat{\mathbf{v}}_K$, then by multiplying $e^{-\lambda_K t}$, we can extract the next term as

$$\lim_{t\to\infty} e^{-\lambda_K t} \left[\mathbf{g}\left(f^t(\mathbf{x})\right) - \sum_{j=0}^{K-1} e^{\lambda_j t} \varphi_j(\mathbf{x})\hat{\mathbf{v}}_j \right] = \varphi_K(\mathbf{x})\hat{\mathbf{v}}_K. \tag{4.6}$$

Taking the integral on both sides of (4.6), hence we proved (4.1). □

The GLA computation starts with identifying the largest Koopman eigenvalue associated with the evolution of the observable and removing the manner contributed terms in equation(4.6). However, this leads to an unstable computation and it only works on an attractor with infinite time. An alternative is to DMD, which tries to approximate the Koopman operator with a linear model. That advances the spatial observables from one time to time , but in general finitely many linear observables are not rich enough for many non-linear systems.

4.1 Dynamic Mode Decomposition

Dynamic mode decomposition(DMD) was developed by P.J.Schmid[22], based on snapshots of the flow to yield fluid structures that accurately describe the motion of the flow. Rowley et al.[21] established the first connection between DMD and the Koopman operator. DMD is based on the proper orthogonal decomposition (POD), and to reduce the computational efficiency, we use singular value decomposition (SVD). In contrast to SVD, DMD provides a modal decomposition in which each mode is composed of spatially correlated structures with the same linear time behaviour. Thus, DMD is also capable of dimensionality reduction by reducing the set of modes and provides a model to analyses these modes evolve in time.

Several factors have contributed to the widespread adoption of DMD as the algorithm of choice for processing high-dimensional spatiotemporal data. The DMD algorithm approximates the best-fit linear matrix operator that advances the high-dimensional observables of a system in time. Thus, DMD approximates the Koopman operator constrained to the subspace of direct observables of the state of a system. DMD applies to both experimental and simulated data because it relies solely on observable data and does not require knowledge of the governing equations.

Definition 4.1 (Standard DMD[22])**.** Consider a sequential set of data vectors $\{\mathbf{z_0}, \ldots, \mathbf{z}_m\}$, where each $\mathbf{z}_k \in \mathbb{R}^n$. We assume that the data are generated by linear dynamics

$$\mathbf{z}_{k+1} = \mathbf{A}\mathbf{z}_k, \tag{4.7}$$

for some (unknown) matrix $\mathbf{A}$. Alternatively, the data could be generated by a continuous time $\mathbf{z}(t)$ with $\mathbf{z}_k = \mathbf{z}(k\Delta t)$ with a fixed timestep Δt. When DMD is applied to non-linear dynamics, we assume that there is an operator $\mathbf{A}$ which approximates those dynamics. and we use DMD to approximate the eigenvectors and eigenvalues of the operator $\mathbf{A}$, where the DMD modes are the eigenvectors and DMD eigenvalues are the eigenvalues of $\mathbf{A}$.

Algorithm 1 Standard DMD[24]

Input: a data set of vectors $\{\mathbf{z_0}, \ldots, \mathbf{z}_m\}$, where each $\mathbf{z}_k \in \mathbb{R}^n$.

1. Arrange the data $\{\mathbf{z_0}, \ldots, \mathbf{z}_m\}$ into matrices

$$\mathbf{X} \triangleq [\mathbf{z_0}, \ldots, \mathbf{z}_{m-1}], \quad \mathbf{Y} \triangleq [\mathbf{z_1}, \ldots, \mathbf{z}_m] \tag{4.8}$$

2. Compute the reduced SVD of $\mathbf{X}$

$$\mathbf{X} = \mathbf{U}\mathbf{\Sigma}\mathbf{V}^*, \tag{4.9}$$

where $\mathbf{U} \in \mathbb{C}^{n\times r}$, $\mathbf{\Sigma} \in \mathbb{C}^{r\times r}$, and $\mathbf{V} \in \mathbb{C}^{m\times r}$ and $r \leq m$ denotes the rank of the data matrix $\mathbf{X}$

3. Define the matrix

$$\mathbf{A} \triangleq \mathbf{U}^*\mathbf{Y}\mathbf{V}\mathbf{\Sigma}^{-1}. \tag{4.10}$$

4. Compute eigenvalues and eigenvectors of $\tilde{A}$,

$$\mathbf{A}\mathbf{w} = \lambda\mathbf{w} \tag{4.11}$$

5. Compute the DMD modes $\hat{v}$ corresponding to λ,

$$\mathbf{v} \triangleq \mathbf{U}\mathbf{w}. \tag{4.12}$$

The standard DMD assumes a sequential set of data vectors $\{\mathbf{z_0}, \ldots, \mathbf{z}_m\}$, so the orders of vector $\mathbf{z}_k$ is important, and $\mathbf{z}_k$ satisfies the relation in equation(4.7), imposing too

many restrictions on A. As a result, in 2014, exact dynamic mode decomposition(Exact DMD) was developed by [24], which works for non-sequential data and we can concatenate multiple different time series into one data matrix. Consider a collection of data pairs $\{(\mathbf{x}(t_k), \mathbf{x}(t_{k+\Delta t}))\}_{k=1}^{m}$. For Exact DMD we don't need the time t_k to be sequential, but we need each snapsot $\mathbf{x}(t_{k+\Delta t})$ is one time step Δt further than the corresponded snapshot $\mathbf{x}(t_k)$. These snapshots are arrange into two data matrices $\mathbf{X}$ and $\mathbf{Y} \in \mathbb{R}^{n\times m}$,

$$\mathbf{X} = \begin{bmatrix} | & | & & | \\ \mathbf{x}(t_1) & \mathbf{x}(t_2) & \cdots & \mathbf{x}(t_m) \\ | & | & & | \end{bmatrix}, \tag{4.13}$$

$$\mathbf{Y} = \begin{bmatrix} | & | & & | \\ \mathbf{x}(t_{1+\Delta t}) & \mathbf{x}(t_{2+\Delta t}) & \cdots & \mathbf{x}(t_{m+\Delta t}) \\ | & | & & | \end{bmatrix}. \tag{4.14}$$

To apply this method to the standard DMD method, we assume that

$$\mathbf{Y} = \mathbf{A}\mathbf{X} \tag{4.15}$$

for some unknown matrix $\mathbf{A}$.

Definition 4.2 (Exact DMD[24])**.** For a dataset given by equation (4.13), define the matrix

$$\mathbf{A} \triangleq \mathbf{Y}\mathbf{X}^{\dagger}, \tag{4.16}$$

where $\mathbf{X}^{\dagger}$ is the pseudo-inverse of $\mathbf{X}$. The DMD of the pair $(\mathbf{X}, \mathbf{Y})$ is given by the eigen-decomposition of $\mathbf{A}$. That is, the DMD modes and eigenvalues are the eigenvectors and eigenvalues of $\mathbf{A}$.

Remark 1. The best fitting matrix $\mathbf{A}$ establishes a linear dynamical system that advances snapshot observables approximately in time, which can be expressed as an optimisation problem

$$\mathbf{A} = \arg\min_{\mathbf{A}} \|\mathbf{Y} - \mathbf{A}\mathbf{X}\|_F = \mathbf{Y}\mathbf{X}^{\dagger}, \tag{4.17}$$

where $||\cdot||_F$ denotes the Frobenius norm. The pseudo-inverse is computed using the reduced SVD of $\mathbf{X} = \mathbf{U}\mathbf{\Sigma}\mathbf{V}^*$ as $\mathbf{X}^{\dagger} = \mathbf{V}\mathbf{\Sigma}^{-1}\mathbf{U}^*$. The matrices $\mathbf{U} \in \mathbb{C}^{n\times m}$ and $\mathbf{V}^{m\times m}$ are unitary, so that $\mathbf{U}^*\mathbf{U} = \mathbf{I}$ and $\mathbf{V}^*\mathbf{V} = \mathbf{I}$, where * denotes complex-conjugate transpose. The columns of $\mathbf{U}$ are known as POD modes as in [23].

Definition 4.3. (Linear consistency [24]) Two matrices $\mathbf{X}, \mathbf{Y} \in \mathbb{R}^{n\times m}$ are *linearly consistent* if and only if the nullspace of $\mathbf{Y}$ contains the nullspace of $\mathbf{X}$.

Here X is the initial state of the dynamics, and Y is the state after the flow time Δt in a dynamical system $\mathbf{x}_{k+1} = f(\mathbf{x}_k)$ such that $\mathbf{Y} = f(\mathbf{X})$.

Algorithm 2 Exact DMD for KMD

Input: initial state $\mathbf{X} = [\mathbf{x}(t_1)\cdots\mathbf{x}(t_m)]$, $\mathbf{x}(t_k) \in \mathbb{R}^n, k = 1,,,m$, the flow map $f(\mathbf{x})$, the observable function $\mathbf{g}(\mathbf{x})$ and the time step Δt

1. Define $\mathbf{Y} = f(\mathbf{X})$
2. Define observations of $\mathbf{X}$ and $\mathbf{Y}$

$$\begin{aligned} \mathbf{\Psi}^0 &= \mathbf{g}(\mathbf{X}) \\ \mathbf{\Psi}^{\Delta t} &= \mathbf{g}(\mathbf{Y}) \end{aligned} \tag{4.18}$$

3. Compute the reduced SVD of $\mathbf{\Psi}^0$ such that

$$\mathbf{\Psi}^0 = \mathbf{U}\mathbf{\Sigma}\mathbf{V}^*, \tag{4.19}$$

where $\mathbf{U} \in \mathbb{C}^{n\times r}$, $\mathbf{\Sigma} \in \mathbb{C}^{r\times r}$, and $\mathbf{V} \in \mathbb{C}^{m\times r}$ and $r \leq m$ denotes the rank of the data matrix $\mathbf{X}$.

4. Define the matrix

$$\mathbf{A} \triangleq \mathbf{U}^*\mathbf{\Psi}^{\Delta t}\mathbf{V}\mathbf{\Sigma}^{-1}. \tag{4.20}$$

5. Compute eigenvalues and eigenvectors of $\tilde{A}$,

$$\mathbf{A}\mathbf{w} = \lambda\mathbf{w} \tag{4.21}$$

6. Compute the DMD modes $\hat{\mathbf{v}}$ corresponding to λ as

$$\hat{\mathbf{v}} \triangleq \frac{1}{\lambda}\mathbf{Y}\mathbf{V}\mathbf{\Sigma}^{-1}\mathbf{w}. \tag{4.22}$$

Remark 2. When $m \ll n$, we can modify the algorithm to reduce the computational cost on $\mathbf{A}$ as it will have at most m non-zero eigenvalues and non-trivial eigenvectors. In practice, the rank of $\mathbf{A}$ may been even lower, given by $r \leq m$. Instead of computing $\mathbf{A}$ in equation (4.20), we can project $\mathbf{A}$ on to the first r POD modes in U_r and use the rank r SVD approximation on $\mathbf{X} \approx \mathbf{U}_r\mathbf{\Sigma}_r\mathbf{V}_r^*$ to compute the approximate $\tilde{\mathbf{A}}$.

4.2 Koopman Spectral Analysis

When the DMD modes and eigenvalues are computed by Algorithm 2, we can represent the system state in terms of the DMD expansion,

$$\mathbf{x}_k = \sum_{j=1}^{n} a_{jk}\lambda_j^{k-1}\hat{\mathbf{v}}_{\lambda_\mathbf{j}} = \mathbf{\Phi}\Lambda^{k-1}\mathbf{a}^k, \tag{4.23}$$

where $\hat{\mathbf{v}}_{\lambda_j}$ are the eigenvectors of A as the DMD modes, λ_j are the eigenvalues of A corresponds to DMD eigenvalues, and a_j are the DMD mode amplitudes. Comparing equation (4.23) and equation (3.21), we can see that if $\mathbf{X}$ and $\mathbf{Y}$ are linearly consistent, the DMD modes are equivalent to Koopman modes, and the DMD eigenvalues are equivalent to Koopman eigenvalues, where the DMD mode amplitudes a_{jk} are the Koopman eigenfunctions evaluated at the initial condition $\varphi_{\lambda_j}(\mathbf{x}_0)$.

To connect the DMD expansion to the Koopman mode decomposition3.21, we write the KMD explicitly in matrix form for the special observable $\mathbf{g}(\mathbf{x}) = \mathbf{x}$ as

$$\mathbf{x}_k = \sum_{j=1}^{n} \lambda_j^{k-1}\varphi_{\lambda_j}(\mathbf{x}_1)\hat{\mathbf{v}}_{\lambda_\mathbf{j}} = \underbrace{\begin{bmatrix} | & & | \\ \hat{\mathbf{v}}_{\lambda_\mathbf{1}} & \cdots & \hat{\mathbf{v}}_{\lambda_\mathbf{n}} \\ | & & | \end{bmatrix}}_{\mathbf{\Phi}} \underbrace{\begin{bmatrix} \lambda_1 & & \\ & \ddots & \\ & & \lambda_n \end{bmatrix}}_{\mathbf{\Lambda}} \underbrace{\begin{bmatrix} \varphi_{\lambda_1}(\mathbf{x}_1) \\ \vdots \\ \varphi_{\lambda_n}(\mathbf{x}_1) \end{bmatrix}}_{\mathbf{a}^k}. \tag{4.24}$$

Thus, comparing with the DMD expansion 4.23, the correspondence between the terms is clear, making it possible to express the data matrix $\mathbf{X}$ as

$$\mathbf{X} = \begin{bmatrix} | & & | \\ \hat{\mathbf{v}}_{\lambda_1} & \cdots & \hat{\mathbf{v}}_{\lambda_n} \\ | & & | \end{bmatrix} \begin{bmatrix} a_1^k & & \\ & \ddots & \\ & & a_n^k \end{bmatrix} \begin{bmatrix} \lambda_1 & \cdots & \lambda_1^{m-1} \\ \vdots & \ddots & \vdots \\ \lambda_n & \cdots & \lambda_n^{m-1} \end{bmatrix}. \tag{4.25}$$

The DMD mode amplitudes in $\mathbf{a}^k$ are often given by

$$\mathbf{a}^k = \mathbf{\Phi}^\dagger \mathbf{x}_1, \tag{4.26}$$

using the first snapshot to determine the DMD mode amplitudes. Hence the first snapshot of DMD correspond the initial condition for KMD.

The spectral expansion in equation(4.23) can be converted to continuous time by introducing the continuous eigenvalues $\omega_j = \log(\lambda_j)/\Delta t$:

$$\mathbf{x}(t) = \sum_{j=1}^{n} a_{jk} e^{\omega_j t} \hat{\mathbf{v}}_{\lambda_j} = \mathbf{\Phi} \exp(\mathbf{\Omega} t) \mathbf{a}^k, \tag{4.27}$$

where $\mathbf{\Omega}$ is a diagonal matrix containing the continuous-time eigenvalues ω_j.

When we apply Algorithm 2, there is a natural question for everyone, how do we choose the parameters? (i.e., how do we choose the timestep Δt to reduce the error? How do we choose the unknown constant variable in the given dynamical system?) and what impact does the choice of the observables has on our ability to do numerical KMD? In the following example, we will try to answer those questions.

Example 4.1. Apply DMD to Example 3.1,with the initial state $\mathbf{x}$ given by (1,1),(3,3) ,(5,5),(-1,1),(-3,3),(-5,5),(-1,-1),(-3,-3),(-5,-5), we choose $\mu, \lambda < 0$ to keep the system stable.

Let us use the eigen-observables $\mathbf{g}(\mathbf{x}) = (x, y, x^2) = (x_1, x_2, x_1^2)$. We create the data matrix $\mathbf{\Psi}^0$ and $\mathbf{\Psi}^{\Delta t}$ with the flow of the system (3.39) and the observables $\mathbf{g}(\mathbf{x})$, then pass them through Algorithm 2, followed by the computation of t DMD eigenvalues. For the value of λ and μ, we first pick λ to be small, -0.05, and change the values of μ to be $-0.1, -0.5, -1, -2, -5$ and, -10 with different timestep Δt. Then we compare the exact eigenvalues and DMD eigenvalues in the logarithmic scale for the plots to demonstrate the rate of change of the relative error with respect to Δt, and select Δt in logspace to create an array of equally spaced values between two numbers on the logarithmic scale. The result is shown in Figure 4a. We can see that when the value of λ is set, the relative error between the DMD eigenvalue and the exact eigenvalue λ decreases linearly when Δt increases and stays steady after hitting an optimal Δt and keeps steady for a while, then increase. However, this is not true for the eigenvalues μ and 2μ; the relative errors decrease linearly and eventually reach an optimal Δt, increasing exponentially after passing through the optimal point. This suggests the optimal Δt depends on the values of μ as the smaller value of μ corresponds to a more significant value of Δt. Also, we think the first graph may result from the same graph as others if we increase the value of λ. We then increase the value of λ to -12. We change the value of largest μ from -10 to -5.5 as we want $\lambda < 2\mu$, the results in shown in Figure 4b. that when the eigenvalue λ is most significant, it has the same shape as when the eigenvalue is 2μ; the shape of the eigenvalue μ is similar to what we have in the first figure in Figure 4a, and the order of the increasing line is the same as the second figure as the smaller the μ is, the larger the optimal Δt. Now we keep μ to be the same and vary λ; we can see the result in Figure 4c, we can see that there is similar to what we have before in Figure 4a and Figure 4b.

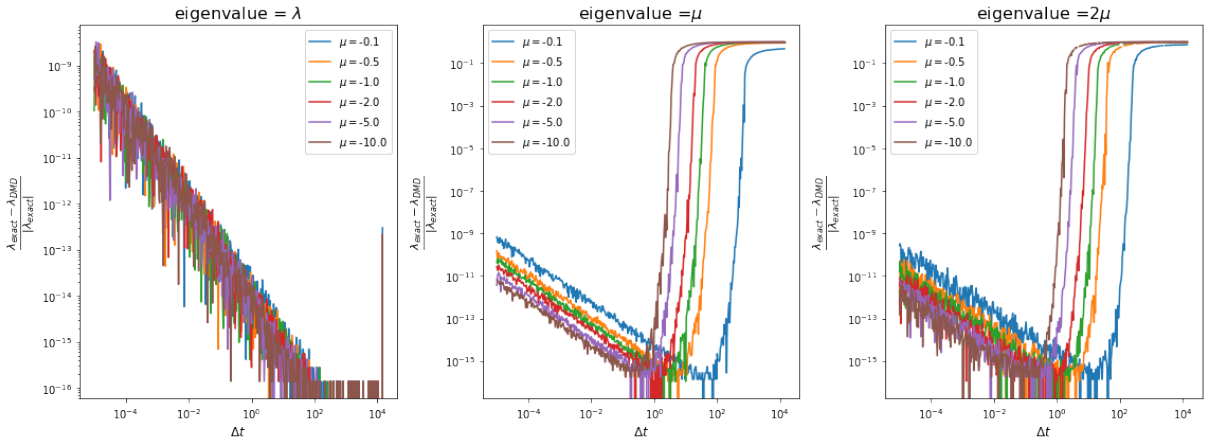

(a) $\lambda = 0.05$

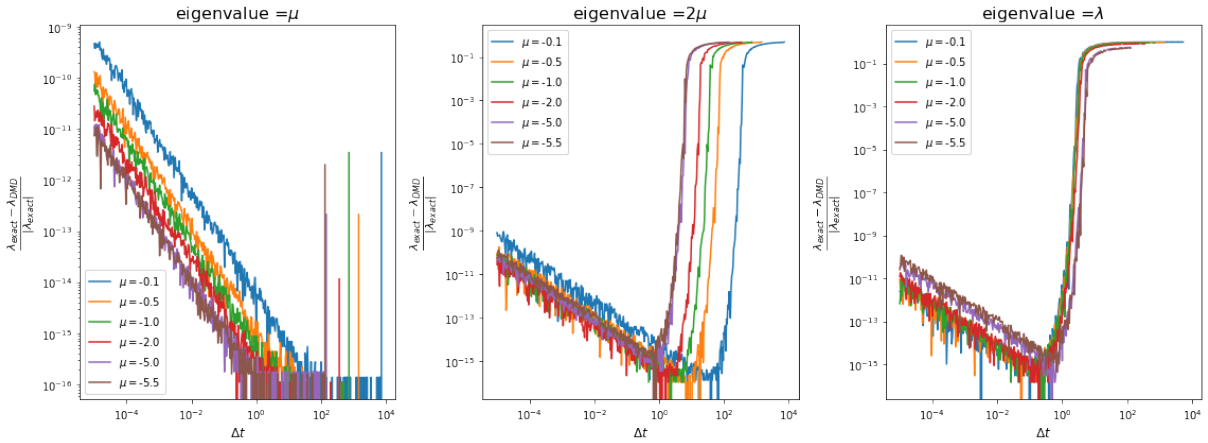

(b) $\lambda = 12$

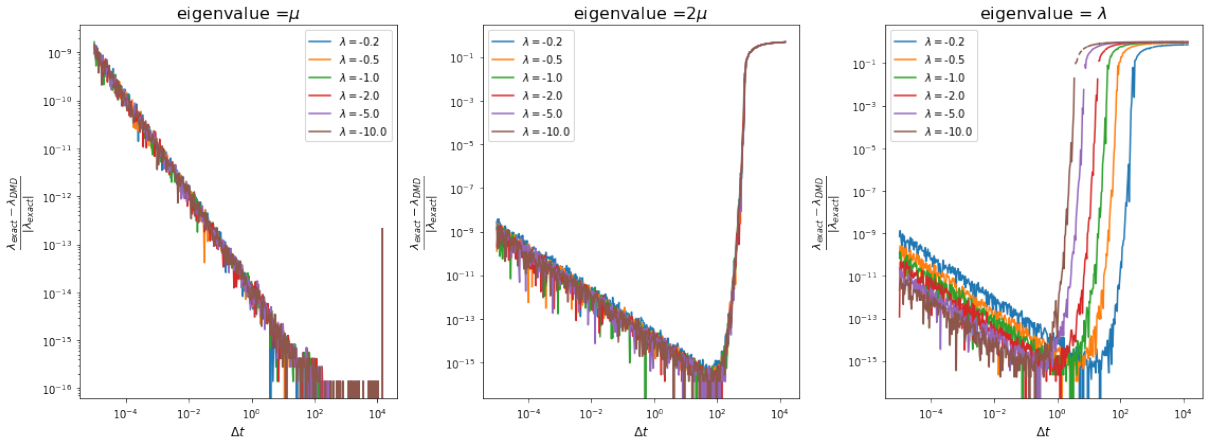

(c) $\mu = 0.05$

Figure 4: The loglog plot for the relative error $\frac{\lambda_{exact}-\lambda_{DMD}}{|\lambda_{exact}|}$ between different values of μ and λ in different Δt that $\Delta t = \text{logspace}[-3, 4]$

This result is interesting, and it shows a correlation between the value of the eigenvalues and the time step Δt affects the relative error so that we can find the minimum relative error; hence we can reduce the error for the DMD. To find the correlation, we now change the scale of the $x - axis$ into $|\lambda_i|\Delta t$ so we can see the correlation between eigenvalues λ and Δt affect the relative error. The result is showed in Figure 5a with $\lambda = -0.05$ and $\mu = -0.1, -0.5, -1, -2, -5$ and -10, we can see that all the curves are overlapping on each others, where we can see the result that the optimal $|\lambda_i|\Delta t$ is in the range $10^{-0.5}$ to 10. To see this more clearly, we enlarge the graph by change the range of Δt into

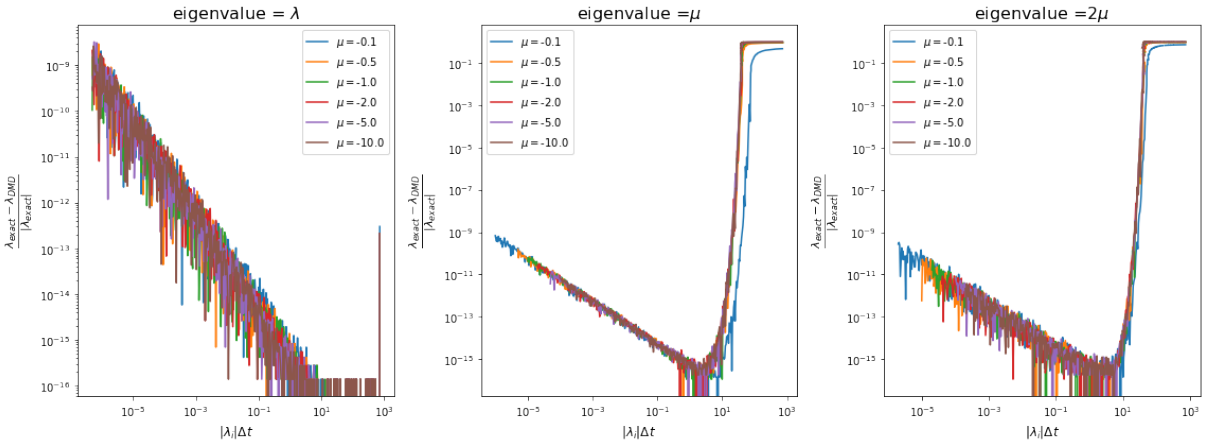

(a) $\Delta t = \text{logspace}[-3, 4]$

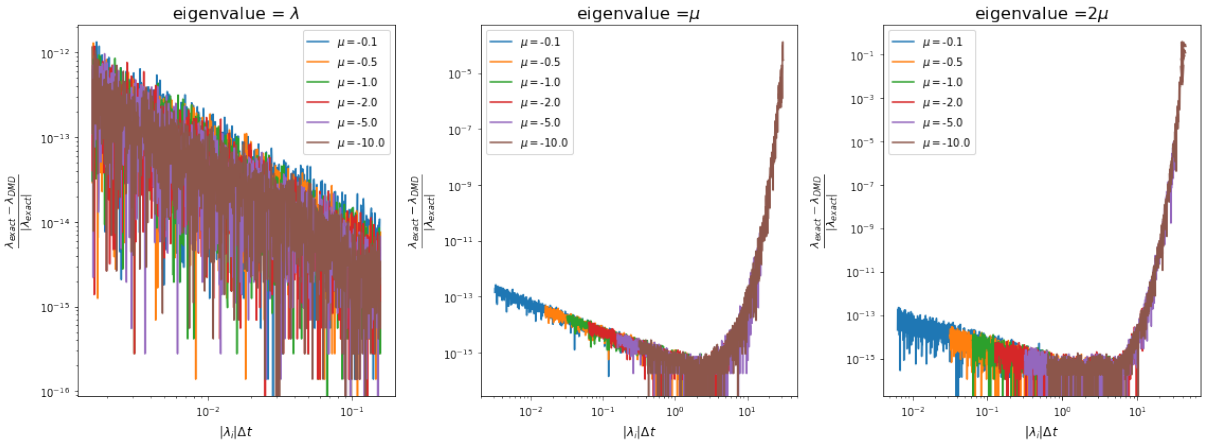

(b) $\Delta t = \text{logspace}[-1.5, 1]$

Figure 5: The loglog plot for the relative error $\frac{\lambda_{exact}-\lambda_{DMD}}{|\lambda_{exact}|}$ and $|\lambda_i|\Delta t$ with $\lambda = -0.05$ and $\mu = -0.1, -0.5, -1, -2, -5$ and -10.

logspace $[-1.5, 1]$ as shown in Figure 5b, and we can see that the optimal point is close to 1 for eigenvalue $= \mu$, and the optimal point is close to 10 for eigenvalue $= 2\mu$, since this is in log scale, so we need to take ln on $|\lambda_i|\Delta t$. Now we find the optimal point for each eigenvalue. However, we want the least relative error on DMD, so we need to sum all the errors together with $x - axis$ being the largest eigenvalue times with the Δt; the reason we use the largest absolute eigenvalue is that if we look at the right figure in Figure 5b, the relative error for 2μ is about 10^{-1}, but for μ, the relative error is about 10^{-5}, the difference between those two is huge, and this shows that the largest absolute eigenvalue dominant the relative errors, therefore when we plot the sum error, we use the largest eigenvalue times the Δt.

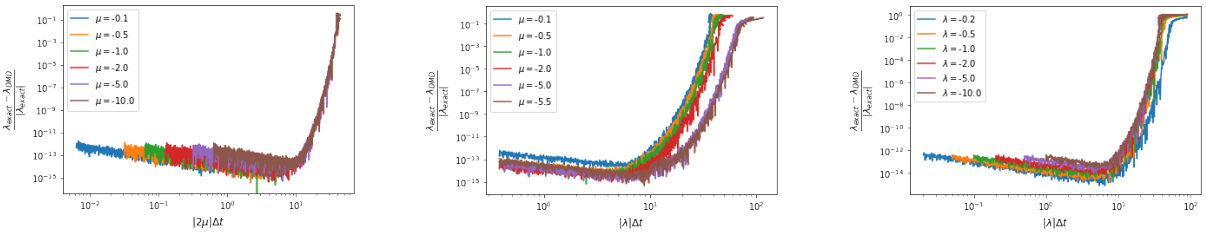

(a) $\lambda = 0.05$ (b) $\lambda = 12$ (c) $\mu = 0.05$

Figure 6: The loglog plot for the sum of the relative errors $\frac{\lambda_{exact}-\lambda_{DMD}}{|\lambda_{exact}|}$ and the smallest eigenvalue multiply with Δt, $\Delta t = \text{logspace}[-1.5, 1]$

The result shown in Figure 6, and we plot the three cases as in Figure 4, and use the largest eigenvalue times Δt as the $x - axis$, we can see that the optimal point in here satisfy the correlation that we need $\ln(\max\{|\lambda_i|\}\Delta t) \in [1, 10]$ and as close to 10 as possible.

Example 4.2. Use the same non-linear system from Example 3.1, we first use initial point (1,1), with $\lambda = -0.05$ and $\mu = -10$, and we use same time interval $t \in [0, 60]$, from the observation we find in example 4.1 that if we want the error of the eigenvalue to be small, we need $\ln(\max\{|\lambda_i|\}\Delta t) \in [1, 10]$, hence we let $\Delta t = 0.6$. Same as above, we first create our data matrix $\mathbf{\Psi}^0$ and $\mathbf{\Psi}^{\Delta t}$, we use the modes and eigenvalues computed by the Algorithm 2 and the observable functions to compute KMD, hence we can simulate the the flow of the non-linear system(3.39) with the observable function $\mathbf{g}(\mathbf{x}) = (x_1, x_2, x_1^2)$. In Figure 7, We plot the exact flow and the flow computed by DMD; we can see that they are identical, and the error decreases when the time t increasing; the reason this happens is when t goes to large, the flow is flowing to the fixed point, the origin, so points are getting smaller and closer to each point, so the error is decreasing when the flow very close to 0, and the difference between each iteration are minimal. The result shows that we can use DMD to simulate the flow of a non-linear system with finite observables.

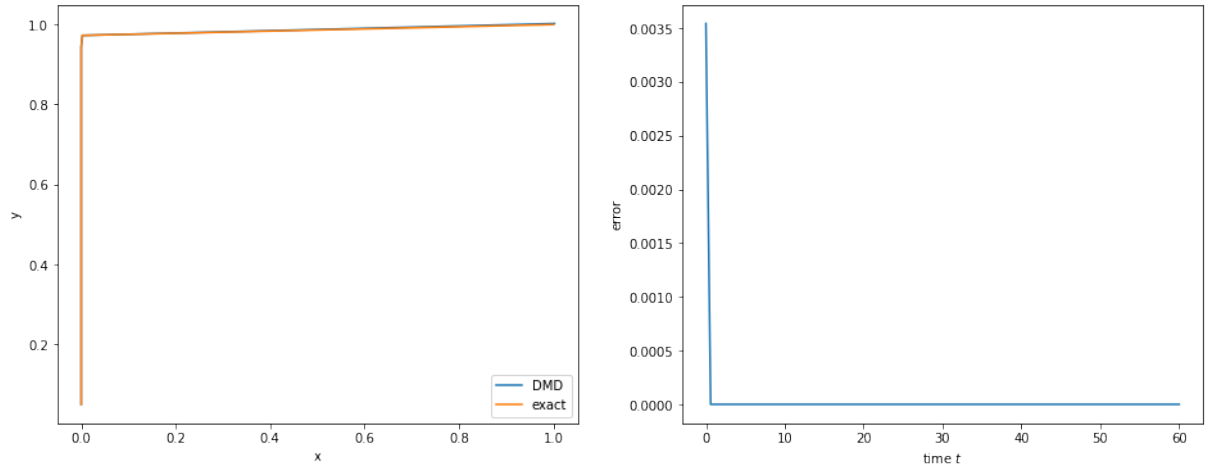

Figure 7: The flow of the non-linear system 3.39 against the flow computed by DMD and the error between the exact flow and the DMD with the initial point $(1, 1)$ and time $t = 60$ with $\Delta t = 0.6$

Now, use DMD on to another observable function $\mathbf{g}(\mathbf{x}) = e^{\mathbf{x}}$, same as in Example 3.1, We first create the data matrix $\mathbf{\Psi}^0$ and $\mathbf{\Psi}^{\Delta t}$ and use Taylor expansion to the $\mathcal{K}^t(\mathbf{g}(\mathbf{x}))$ and choose the first 5 terms of the Taylor expansion as our observable function to input into the DMD algorithm. We use $\lambda = -0.05$, $\mu = -1$ and time $t = 60$ with $\Delta t = 0.15$, the initial point is $(1, 1)$. In Figure 8a, we plotted the real part of the exact eigenvalues in the blue horizontal line, the DMD eigenvalues in the red circle, and the exact eigenvalues in the blue dot. We can see that three red circles are not matched with any blue line, and two DMD eigenvalues are with imaginary parts. If we enlarge the part where all the blue dot and red circle overlapping, as shown in Figure 8b, we can see that there are some lines are thicker than the others because of the repeated eigenvalues, and most of the red circles and blue dot are matched, but there is one miss matched at -2.15, we can see that overall the DMD gives out mostly correct eigenvalues but contains duplication. In total, four DMD eigenvalues are incorrect compared to exact eigenvalues; this is because we have four repeated exact eigenvalues, and the DMD cannot deal with repeated eigenvalues as it requires the empirical Ritz values λ_j are distinct [21]. So one limitation of the DMD algorithm is to handle the repeated eigenvalues.

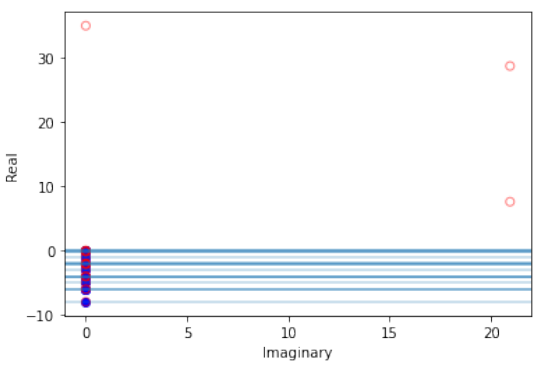

(a) All the exact and DMD eigenvalues

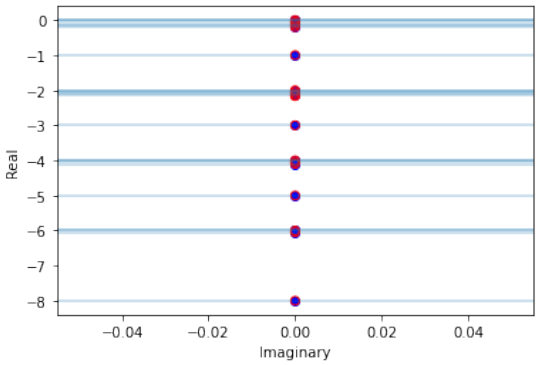

(b) Part of exact and DMD eigenvalues

Figure 8: The comparison of exact eigenvalues and DMD eigenvalues, with $\mu = -1$ and $\lambda = -0.05$ the blue horizontal line is the real part of the exact eigenvalues, The blue dot is the exact eigenvalues and the red circle is the DMD eigenvalues. (a) We plotted all the exact and DMD eigenvalues. (b) We plotted the part without three outer DMD eigenvalues and the non-repeated exact eigenvalues.

In summary, we introduced numerical methods for Koopman mode analysis and the DMD algorithm. We applied DMD to the non-linear system, and empirical data shows the relationship between the largest absolute eigenvalue and the time step Δt is $\ln(\max\{|\lambda_i|\}\Delta t) \in [1, 10]$ to reduce the error of the DMD. Also, we show that Koopman mode analysis numerical methods work for the non-linear dynamical system. However, DMD is fundamentally unstable to tackle the linear dynamical system with the multiple fixed point[3]. Then, we would like to imply this on non-linear PDEs to verify if this works too.

5 Burgers Equation

In 1948, J. M. Burgers[5] proposed a non-linear PDE as a way of modelling the turbulence in fluids, so the general form of the one-dimensional Burgers equation is

$$\frac{\partial u}{\partial t} + u\frac{\partial u}{\partial x} = \nu\frac{\partial^2 u}{\partial x^2}, \tag{5.1}$$

where u represents the velocity of the fluid and ν is the viscosity of fluid. Hopf[11] and Cole [6] obtained an analytic solution for it by the method change of variables to transform equation(5.1) into a linear diffusion equation, for which solutions can be computed easily from Fourier transforms. This technique is named as the Cole-Hopf transformation. However, the Burgers equation has proven to be an inadequate model for fluid turbulence, and it remains a topic of active research to this day.

In [20], Jacob showed that we can apply Koopman analysis on Burgers equation with with Dirichlet boundary conditions, and connect this with DMD so that we can simulate the flow of the Burgers equation. Follow the same condition in [20], we consider the Burgers equation over a domain of length L with Dirichlet boundary conditions $u\left(-\frac{L}{2}, t\right) = u\left(\frac{L}{2}, t\right) = 0$, with $L = 6\pi$ and $\nu = 0.1$, which is equivalent to a Reynolds number $\mathrm{Re} = 60\pi$ on a unit-length domain. We solve equation(5.1) subject to a given initial condition $u(x, 0) = u_0(x)$.

5.1 Cole-Hopf Transformation

The Cole-Hopf transformation consists of two steps. First, we use the method change of variables that we define a new variable $\psi(x, t)$ that

$$u = \frac{\partial \psi}{\partial x} \tag{5.2}$$

Substituting this into equation(5.1) yields

$$\frac{\partial}{\partial t}\frac{\partial \psi}{\partial x} + \frac{\partial \psi}{\partial x}\frac{\partial^2 \psi}{\partial x^2} = \nu\frac{\partial^3 \psi}{\partial x^3}, \tag{5.3}$$

$$\implies \frac{\partial}{\partial x}\left(\frac{\partial \psi}{\partial t} + \frac{1}{2}\left(\frac{\partial \psi}{\partial x}\right)^2 - \nu\frac{\partial^2 \psi}{\partial x^2}\right) = 0. \tag{5.4}$$

which implies that the sum in the brackets is independent of x, implying that it can only be a function of t. Because of the boundary conditions, this function must be identically zero. So we have

$$\frac{\partial \psi}{\partial t} + \frac{1}{2}\left(\frac{\partial \psi}{\partial x}\right)^2 - \nu\frac{\partial^2 \psi}{\partial x^2} = 0. \tag{5.5}$$

Second, we change of variables $v(x, t)$ again

$$\psi(x, t) = -2\nu \ln(v(x, t)), \tag{5.6}$$

the derivatives of ψ are given in terms of v by

$$\frac{\partial \psi}{\partial t} = -\frac{2\nu}{v}\frac{\partial v}{\partial t}, \quad \frac{\partial \psi}{\partial x} = -\frac{2\nu}{v}\frac{\partial v}{\partial x}, \quad \frac{\partial^2 \psi}{\partial x^2} = \frac{2\nu}{v^2}\left(\frac{\partial v}{\partial x}\right)^2 - \frac{2\nu}{v}\frac{\partial^2 v}{\partial x^2}, \tag{5.7}$$

which are substituted into equation(5.5) and cancellation of the non-linear terms yields are noted.

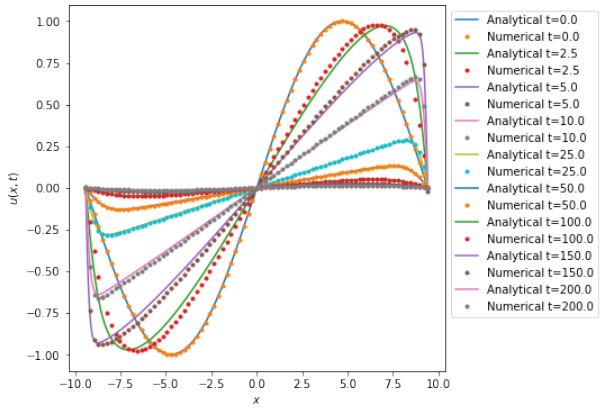

Figure 9: Evolution of $u_0(x) = \sin\left(\frac{2\pi x}{L}\right)$ for $t \leq 200$, The line is computed by analytic solution, the dot is computed by finite difference method.

$$\frac{\partial v}{\partial t} = \nu \frac{\partial^2 v}{\partial x^2}. \tag{5.8}$$

This linear equation is known as the diffusion equation. Then we have

$$u(x,t) = -\frac{2\nu v_x}{v}. \tag{5.9}$$

Integrating with respect to x we will obtain the following result

$$v(x,t) = C(t) \exp\left(-\frac{1}{2\nu} \int_{-\frac{L}{2}}^{x} u(\tau, t)\, d\tau\right), \tag{5.10}$$

where $C = v(-\frac{L}{2}, t)$. The initial values are simply related. If

$$u(x,0) = u_0(x), \tag{5.11}$$

then

$$v(x,0) = v_0(x) = C_0 \exp\left(-\frac{1}{2\nu} \int_{-\frac{L}{2}}^{x} u_0(\tau)\, d\tau\right), \tag{5.12}$$

Now Let us take the initial condition as a sine wave $u_0(x) = \sin\left(\frac{2\pi x}{L}\right)$, see Figure 9, we used two methods to compute the solution of the Burgers equation, Fourier series and finite difference method.

5.2 Solve Burgers Equation via Finite difference

We apply Euler method to solve the Burgers equation. We all know that Euler method is only first order convergent, i.e, the error pf the computed solution is $\mathcal{O}(\Delta t)$, where Δt is the time step. This is numerically unstable, which causes inaccurate results and requires a small step size to achieve high accuracy. In [1], they show that the importance of picking up correct step size Δt and indicate that we need $\Delta t < \frac{\nu(\Delta x)^2}{2}$.

Consider a standard implicit Euler method for equation(5.1) on the interval $\left(-\frac{L}{2}, \frac{L}{2}\right)$ with initial condition $u(x,0) = \sin\left(\frac{2\pi x}{L}\right)$ with Dirichlet boundary conditions $u\left(-\frac{L}{2}, t\right) = u\left(\frac{L}{2}, t\right) = 0$:

$$\begin{aligned} x_i &= i\Delta x, \qquad i = 0, 1, 2, ..., N, \quad \Delta x = \frac{L}{N}, \\ t_j &= j\Delta t, \qquad j = 0, 1, 2, ..., \end{aligned}$$

and, in a standard notation, define the approximation

$$u_i^j \approx u(x_i, t_j), \qquad i = 0, 1, 2, ..., N, \quad j = 0, 1, 2, ...$$
$$u_i^0 = \sin\left(\frac{2\pi x_i}{L}\right), \quad u_0^j = u_N^j = 0.$$

So we have

$$\frac{u_i^{j+1} - u_i^j}{\Delta t} + \frac{(u_{i+1}^j)^2 - (u_{i-1}^j)^2}{2\Delta x} = \nu \frac{u_{i+1}^j - 2u_i^j + u_{i-1}^j}{(\Delta x)^2}, \tag{5.13}$$

and let $\kappa = \frac{\Delta t}{2\Delta x}$ and $\gamma = \frac{\nu \Delta t}{(\Delta x)^2}$. Then we have

$$u_i^{j+1} = u_i^j - \kappa((u_{i+1}^j)^2 - (u_{i-1}^j)^2) + \gamma(u_{i+1}^j - 2u_i^j + u_{i-1}^j), \tag{5.14}$$

with $u_{-1}^j = u_1^j$ and $u_{N-1}^j = u_{N+1}^j$.

5.3 Solve Burgers Equation via Fourier series

We use spectral analysis on the solution of the equation(5.8) $v(x,t)$. Since we have equation(5.8) and the boundary condition $v_x\left(-\frac{L}{2}, t\right) = v_x\left(\frac{L}{2}, t\right) = 0$, by Separation of variables, we can define

$$v(x,t) = X(x)T(t), \tag{5.15}$$

where $X(x)$ is a function of x and $T(t)$ is a function of t, and then bring it into the diffusion equation, we can obtain the following result

$$X(x)T'(t) = \nu X''(x)T(t) \to \frac{T'(t)}{\nu T(t)} = \frac{X''(x)}{X(x)}, \tag{5.16}$$

since the left hand side only depends on t and the right hand side only depends on x, so both sides are equal to some constant $-\lambda$. We can rewrite this as

$$X''(x) + \lambda X(x) = 0, \tag{5.17a}$$
$$T'(t) + \nu\lambda T(t) = 0. \tag{5.17b}$$

So we solve the first equation for $X(x)$ now, bring in the boundary condition of the equation(5.8), we have

$$\begin{aligned} v_x\left(-\frac{L}{2}, t\right) = X'\left(-\frac{L}{2}\right)T(t) = 0 \to X'\left(-\frac{L}{2}\right) = 0, \\ v_x\left(\frac{L}{2}, t\right) = X'\left(\frac{L}{2}\right)T(t) = 0 \to X'\left(\frac{L}{2}\right) = 0. \end{aligned} \tag{5.18}$$

By solving equation(5.17a) with above boundary condition we have the eigenvalue $\lambda_n = \left(\frac{n\pi}{L}\right)^2$, Hence we have the eigenfunction

$$X_{\lambda_n}(x) = \hat{v}_{\lambda_n}(x) = \begin{cases} \cos\left(\frac{n\pi x}{L}\right) & n \text{ even}, \\ \sin\left(\frac{n\pi x}{L}\right) & n \text{ odd}. \end{cases} \tag{5.19}$$

For each n, the corresponding equation for $T(t)$ becomes

$$T'(t) + \nu\left(\frac{n\pi}{L}\right)^2 T(t) = 0. \tag{5.20}$$

Solve this ODE we have $T(t) = A_n e^{-\nu\left(\frac{n\pi}{L}\right)^2 t}$. Hence we have

$$v_{\lambda_n}(x,t) = X_{\lambda_n}(x)T_{\lambda_n}(x) = A_n e^{-\nu\left(\frac{n\pi}{L}\right)^2 t}\hat{v}_{\lambda_n}(x). \tag{5.21}$$

Hence, by the principle of superposition, we can have the spectral analysis form of $v(x,t)$,

$$v(x,t) = A_0 + \sum_{n=1}^{\infty} A_n e^{-\nu\left(\frac{n\pi}{L}\right)^2 t}\hat{v}_{\lambda_n}(x). \tag{5.22}$$

Now, to find A_0 and A_n, we bring the initial condition equation(5.12) into equation(5.22), and we write $v_0(x)$ as a Fourier series, we obtain:

$$A_0 = \frac{1}{L}\int_{-\frac{L}{2}}^{\frac{L}{2}} v_0(x)dx = \frac{C_0}{L}\int_{-\frac{L}{2}}^{\frac{L}{2}} \exp\left(-\frac{1}{2\nu}\int_0^x u_0(\tau)d\tau\right)dx,$$

$$A_n = \begin{cases} \dfrac{2}{L}\displaystyle\int_{-\frac{L}{2}}^{\frac{L}{2}} v_0(x)\cos\left(\frac{n\pi x}{L}\right)dx = \frac{2C_0}{L}\int_{-\frac{L}{2}}^{\frac{L}{2}} \exp\left(-\frac{1}{2\nu}\int_0^x u_0(\tau)d\tau\right)\cos\left(\frac{n\pi x}{L}\right)dx, & n \text{ even}, \\ \dfrac{2}{L}\displaystyle\int_{-\frac{L}{2}}^{\frac{L}{2}} v_0(x)\sin\left(\frac{n\pi x}{L}\right)dx = \frac{2C_0}{L}\int_{-\frac{L}{2}}^{\frac{L}{2}} \exp\left(-\frac{1}{2\nu}\int_0^x u_0(\tau)d\tau\right)\sin\left(\frac{n\pi x}{L}\right)dx, & n \text{ odd}. \end{cases} \tag{5.23}$$

Hence we can write the solution from equation(5.9)

$$u(x,t) = \frac{2\nu\pi}{L}\frac{\sum_{n=1}^{\infty}(-1)^n A_n e^{-\nu\left(\frac{n\pi}{L}\right)^2 t} n\hat{v}'_{\lambda_n}(x)}{A_0 + \sum_{n=1}^{\infty} A_n e^{-\nu\left(\frac{n\pi}{L}\right)^2 t}\hat{v}_{\lambda_n}(x)} \tag{5.24}$$

We use Python to implement both numerical and analytic solutions of Burgers equation, and we use $\Delta t = 0.0004$ to improve the accuracy of Euler's method in the numerical solution. We also use the trapezoidal rule to simulate an integral part of A_0 and A_n, so that we could save lots of computation time and improve the accuracy, we used $N = 400$ partition to solve those integrals. In Figure 9, we plotted the evolution of $u_0(x) = \sin\left(\frac{2\pi x}{L}\right)$ with the finite difference method and spectral analysis method; we can see the difference between two waves are slight, and there is a small gap between two lines when $t = 2.5$ and $t = 5$, this may be because of the inaccurate of the Euler method, but overall we can verify that the analytic solution of Burgers equation is correct and we will use this as the input of the DMD algorithm and show results in Section 5.5.

5.4 Solve Burgers Equation via Koopman Mode Decomposition

Firstly, Let us use Koopman mode decomposition to solve the Burgers equation via Cole-Hopf equation. Jacob [20] shown that we can use spectral analysis on the diffusion equation, hence we can associated it with Koopman operator.

Define a Koopman mode expansion of $v(u;x)$ such that

$$v(u;x) = \sum_{n=0}^{\infty} \varphi_n(u)\hat{v}_n(x), \tag{5.25}$$

where the dependence on u via the Koopman eigenfunctions φ_n and x via the Koopman modes $\hat{v}_n$ is separated. By the definition of Koopman eigenfunctions we have $\mathcal{K}^t\varphi_n(u) = \varphi_n(u)e^{\lambda_n t}$ and the linearity of the diffusion equation, We use the linearity property of the Koopman eigenfunction and compare the coefficient of the Koopman eigenfunction and equation(5.21), we can see that the Koopman mode $\hat{v}_n(x)$ is the eigenfunction of

the one-dimensional Laplacian. And the Koopman eigenfunction required to evolve v are then

$$\varphi_n(u) = \langle \hat{v}_n(x), v(u;x) \rangle, \tag{5.26}$$

where $\langle f, g \rangle := \frac{2}{L} \int_{-\frac{L}{2}}^{\frac{L}{2}} f g dx$, so that the observable evolved in time is

$$\mathcal{K}^t v(u;x) = \sum_{n=0}^{\infty} \varphi_n(u) e^{\lambda_n t} \hat{v}_n(x), \tag{5.27}$$

where $\lambda_n = -\nu \left(\frac{n\pi}{L}\right)^2$.

Now define the Koopman mode decomposition for $u(x,t)$,

$$u(x,t) = \sum_{n=0}^{\infty} \Phi_n(u) e^{\Lambda_n t} \hat{u}_n(x). \tag{5.28}$$

So at time t, from equation(5.9), we have the Cole-Hopf transformation in the form $uv = -2\nu v_x$, hence we have

$$\sum_{l=0}^{\infty} \sum_{m=0}^{\infty} \Phi_l(u) \varphi_m(u) \hat{u}_l(x) \hat{v}_m(x) e^{(\Lambda_l - \nu\left(\frac{n\pi}{L}\right)^2)t} = -2\nu \sum_{n=0}^{\infty} \varphi_n(u) e^{-\nu\left(\frac{n\pi}{L}\right)^2 t} \hat{v}_n'(x). \tag{5.29}$$

By comparing the coefficient of the exponential terms, we need

$$\Lambda_l - \nu \left(\frac{m\pi}{L}\right)^2 = -\nu \left(\frac{n\pi}{L}\right)^2, \qquad \text{for some } t \tag{5.30}$$

to be satisfied, hence we can determine the Koopman eigenfunction and Koopman mode pairs from above,

$$\sum_{l+m^2=k}^{\infty} \Phi_l(u) \varphi_m(u) \hat{u}_l(x) \hat{v}_m(x) = \begin{cases} -2\nu \varphi_n(u) \hat{v}_n'(x), & k = n^2, \\ 0, & k \neq n^2, \end{cases} \tag{5.31}$$

where $m, n, l, k \in \mathbb{N}$. So we can obtain that the Koopman eigenvalues are $\Lambda_l = -\nu l \left(\frac{\pi}{L}\right)^2$. Hence we can determine the flow of $u(x,t)$,

$$u(x,t) = \sum_{l=0}^{\infty} \Phi_l(u) e^{\Lambda_l t} \hat{u}_l(x) = \begin{cases} \dfrac{-2\nu \varphi_n(u) \hat{v}_n'(x)}{\sum_{l+m^2=k}^{\infty} \varphi_m(u) \hat{v}_m(x)} e^{\Lambda_l t}, & k = n^2, \\ 0, & k \neq n^2. \end{cases} \tag{5.32}$$

5.5 Dynamic Mode Decomposition on Burgers Equation

Let us apply DMD to the solutions of the Burgers equation with the data we produced in Section 5.3. First, we let the observable function $\mathbf{g} = \mathbf{u}$. We can see the result in Figure 10a, and the eigenvalues do not match the analytical solution, which has imaginary parts, so the error grows rapidly after passing the first few DMD eigenvalues. Now we change the observable function to $\mathbf{g} = \mathbf{v}(\mathbf{u})$, and we can see that all the blue dot match with analytic eigenvalues in Figure 10b, but not all; this is because we use the initial condition is a sine wave, which has the symmetry property; hence it can only be determine some of the eigenvalues we have, but this depends on the amplitude of the curve for $u(x)$, as we can see in Figure 9, when $t = 0$, the amplitude of the curve is the highest, so we may be only determine half of the analytic eigenvalues by DMD, as the eigenvalues of

the positive part are same as the negative part, but when $t = 200$, the amplitude of the curve is minimal, and the gradient of the curve is close to 0 which is the fixed point so that we could have more information from that. Here, the elements of the observable vector constitute a suitable basis for the eigenfunctions; thus, DMD successfully extracts the exact eigenvalues for the linearising observable $\mathbf{v}$.

Now we pick the last twenty snapshot pairs as our input and plot the eigenvalues for both observable $\mathbf{g} = \mathbf{u}$ and $\mathbf{g} = \mathbf{v}(\mathbf{u})$ in Figure 11. If we pick the time considerably, we can observe that the first few DMD eigenvalues match the analytical eigenvalues and compare this with Figure 12a . We can see that there are only thirteen incorrect eigenvalues; we think this is because of the repeated eigenvalue from the dynamical system, and that is why we have a conjugate pair of eigenvalues below. If we look for the right figure, we can see that for the observable $\mathbf{g} = \mathbf{v}(\mathbf{u})$,. We can observe that nine DMD eigenvalues match the analytical eigenvalue. When we pick the snapshot pairs from the time interval $t \in [195, 200]$, we can find a few correct DMD eigenvalues and use them to express the full state as they are the dominant term. By taking the experiment with the different interval between $[0, 200]$ with a fixed timestep $\Delta t = 0.5$, the correlation with eigenvalues and timestep in Section 4.2 is not satisfied here as the largest absolute eigenvalue here is infinite, which we cannot measure. As a result, we plotted the graph in Figure 12b where all the eigenvalues in the observation interval $[-0.3, 0]$, we found that we need the time interval at least from $t = 50$ to the end to explore some DMD eigenvalues that match to the analytical eigenvalues, and we can see that if we are increasing the starting time, the gap between the DMD eigenvalues is getting smaller, as we know that the analytical eigenvalues gap should be $\nu \left(\frac{\pi}{L}\right)^2$, and based on the condition we have, that $L = 6\pi, \nu = 0.1$, so the gap is 0.003. Although we can get the matched DMD eigenvalues from the time interval $[50, 200]$, the DMD eigenvalues may not be able to proceed with the KMD correctly. However, this may not apply with other initial conditions or boundary conditions for the same parameters in Burgers equation.

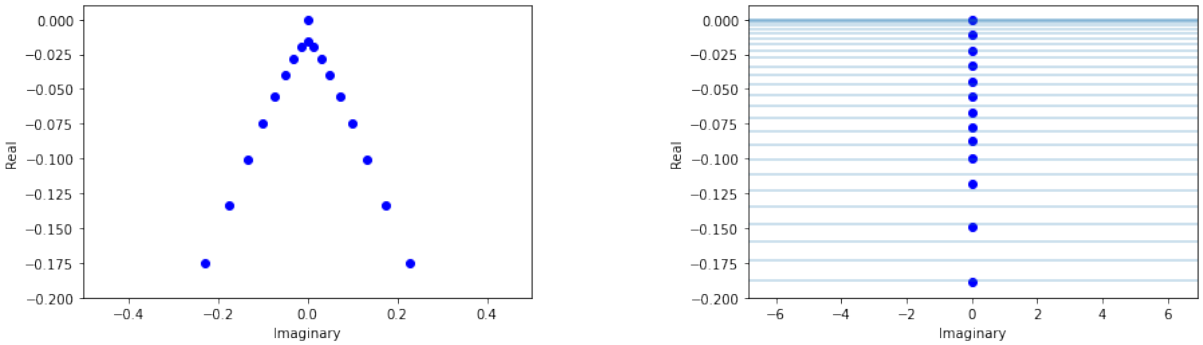

(a) $\mathbf{g} = \mathbf{u}$ (b) $\mathbf{g} = \mathbf{v}(\mathbf{u})$

Figure 10: Eigenvalues from DMD of $u_0(x) = \sin\left(\frac{2\pi x}{L}\right)$ with 400 snapshot pairs with timestep $\Delta t = 0.5$, with the time interval $t \in [0, 200]$ for both $\mathbf{g} = \mathbf{u}$ and $\mathbf{g} = \mathbf{v}(\mathbf{u})$. The blue horizontal lines are the eigenvalues of the linear diffusion problem $-\nu \left(\frac{n\pi}{L}\right)^2$.

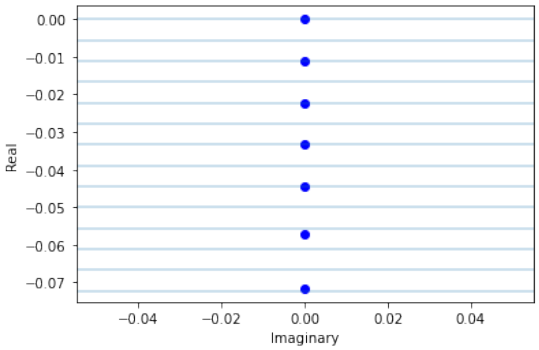

(a) $\mathbf{g} = \mathbf{u}$

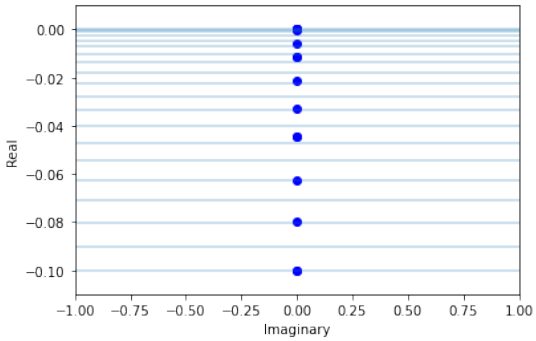

(b) $\mathbf{g} = \mathbf{v}(\mathbf{u})$

Figure 11: First a few eigenvalues from DMD of $u_0(x) = \sin\left(\frac{2\pi x}{L}\right)$ with 20 snapshot pairs with timestep $\Delta t = 0.5$, with the time interval $t \in [190, 200]$ for both $\mathbf{g} = \mathbf{u}$ and $\mathbf{g} = \mathbf{v}(\mathbf{u})$. The blue horizontal lines are the eigenvalues of the linear diffusion problem $-\nu\left(\frac{n\pi}{L}\right)^2$.

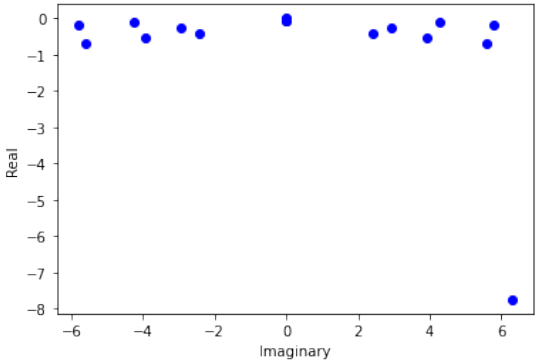

(a)

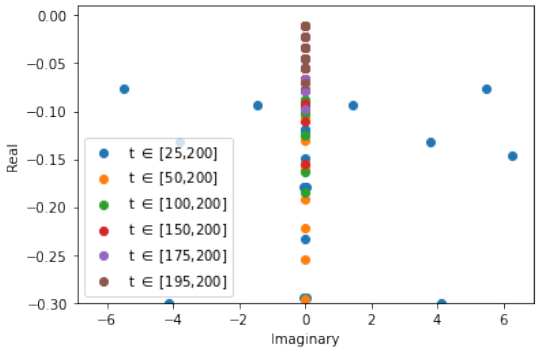

(b)

Figure 12: (a): Eigenvalues from DMD of $u_0(x) = \sin\left(\frac{2\pi x}{L}\right)$ with 20 snapshot pairs with timestep $\Delta t = 0.5$, with the time interval $t \in [195, 200]$ for $\mathbf{g} = \mathbf{u}$. (b): First a few eigenvalues from DMD of $u_0(x) = \sin\left(\frac{2\pi x}{L}\right)$ with timestep $\Delta t = 0.5$, collected within the different time intervals between $25, 50, 100, 150, 175, 195$ to 200 for $\mathbf{g} = \mathbf{u}$.

Next, we change the initial condition into a localised Gaussian pulse $u_0(x) = \exp[-(x + \left(\frac{\pi}{2}\right)^2)]$. Then we apply DMD with different time intervals as used above. The result shown in Figure 13 shows that given the same observation interval, we need $t \in [100, 200]$ to see the first few matched DMD eigenvalues. Moreover, one important difference between the two initial conditions is that the localised Gaussian pulse can derive all the DMD eigenvalues where the sine wave cannot. We showed that a different initial condition might result in a different time interval to observe that the minimum requirement of all the DMD eigenvalues is matched. Furthermore, if we pick the starting time as large as possible, we will obtain that the first few DMD eigenvalues are the analytical eigenvalues.

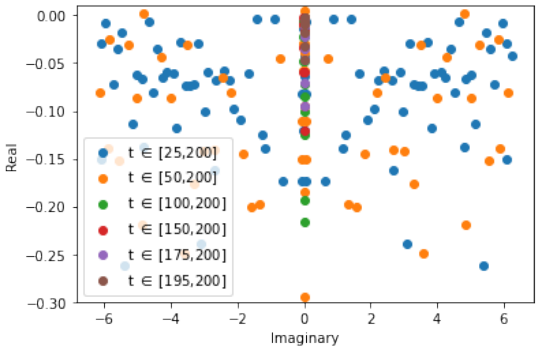

Figure 13: First a few eigenvalues from DMD of $u_0(x) = \exp[-(x + \left(\frac{\pi}{2}\right)^2)]$ with timestep $\Delta t = 0.5$, with the different time intervals between $25, 50, 100, 150, 175, 195$ to 200 for $\mathbf{g} = \mathbf{u}$.

5.6 Burgers Equation with Periodic Boundary Condition

We change the boundary condition from Dirichlet boundary condition into a periodic boundary condition, that we have

$$\begin{cases} \dfrac{\partial u}{\partial t} + u\dfrac{\partial u}{\partial x} = \nu \dfrac{\partial^2 u}{\partial x^2}, \\ u\left(-\dfrac{L}{2}, t\right) = u\left(\dfrac{L}{2}, t\right), \\ u_x\left(-\dfrac{L}{2}, t\right) = u_x\left(\dfrac{L}{2}, t\right). \end{cases} \tag{5.33}$$

From equation(5.9), we know the boundary condition for $v(x,t)$ is periodic boundary condition as well, so we have $v\left(-\frac{L}{2}, t\right) = v\left(\frac{L}{2}, t\right)$ and $v_x\left(-\frac{L}{2}, t\right) = v_x\left(\frac{L}{2}, t\right)$. From equation(5.10), we can see there is a constraint that

$$\int_{-\frac{L}{2}}^{\frac{L}{2}} u(x,t)\, dx = 0. \tag{5.34}$$

Now use the similar method used in Section 5.3, we used Separation of variables and solved the system(5.17), we have the eigenvalue $\lambda_n = \left(\frac{2n\pi}{L}\right)^2$, so we have the eigenfunction

$$X_{\lambda_n}(x) = \hat{v}_{\lambda_n}(x) = e^{\left(\frac{2n\pi xi}{L}\right)} \qquad n = 1, 2, 3, 4, ... \tag{5.35}$$

Hence we can write $v(x,t)$ as

$$v(x,t) = A_0 + \sum_{n=1}^{\infty} A_n e^{\left(\frac{2n\pi xi}{L}\right)} e^{-\nu\left(\frac{2n\pi}{L}\right)^2 t}, \tag{5.36}$$

with

$$\begin{aligned} A_0 &= \frac{1}{L}\int_{-\frac{L}{2}}^{\frac{L}{2}} v_0(x)dx = \frac{C_0}{L}\int_{-\frac{L}{2}}^{\frac{L}{2}} \exp\left(-\frac{1}{2\nu}\int_0^x u_0(\tau)d\tau\right)dx, \\ A_n &= \frac{1}{L}\int_{-\frac{L}{2}}^{\frac{L}{2}} v_0(x)e^{\left(-\frac{2n\pi xi}{L}\right)}dx = \frac{C_0}{L}\int_{-\frac{L}{2}}^{\frac{L}{2}} \exp\left(-\frac{1}{2\nu}\int_0^x u_0(\tau)d\tau\right)e^{\left(-\frac{2n\pi xi}{L}\right)}dx, \end{aligned} \tag{5.37}$$

$$u(x,t) = \frac{4\nu\pi}{L} \frac{\sum_{n=-\infty}^{\infty} niA_n e^{\left(\frac{2n\pi xi}{L}\right)} e^{-\nu\left(\frac{2n\pi}{L}\right)^2 t}}{A_0 + \sum_{n=-\infty}^{\infty} A_n e^{\left(\frac{2n\pi xi}{L}\right)} e^{-\nu\left(\frac{2n\pi}{L}\right)^2 t}} \tag{5.38}$$

Follow the same procedure in Section 5.4, we can write Burgers equation in Koopman mode decomposition. By the Cole-Hopf transformation, we have the following

$$\sum_{l=0}^{\infty}\sum_{m=0}^{\infty} \Phi_l(u)\varphi_m(u)\hat{u}_l(x)\hat{v}_m(x)e^{(\Lambda_l - \nu\left(\frac{2n\pi}{L}\right)^2)t} = -2\nu\sum_{n=0}^{\infty}\varphi_n(u)e^{-\nu\left(\frac{2n\pi}{L}\right)^2 t}\hat{v}_n'(x). \tag{5.39}$$

Hence we have the Koopman eigenfunction and Koopman mode pairs

$$\sum_{l+m^2=k}^{\infty} \Phi_l(u)\varphi_m(u)\hat{u}_l(x)\hat{v}_m(x) = \begin{cases} -2\nu\varphi_n(u)\hat{v}_n'(x), & k = n^2, \\ 0, & k \neq n^2, \end{cases} \tag{5.40}$$

where $m, n, l, k \in \mathbb{N}$. So we can obtain that the Koopman eigenvalues are $\Lambda_l = -4\nu l\left(\frac{\pi}{L}\right)^2$.

We notice that if we pick the initial condition as the sine wave, the solution of the Burgers equation will be the same, as we plotted in Figure 14a, we can see that they are the same. Therefore if we apply DMD to this, the result will be the same as concluded above. However, if we pick the initial condition as a localised Gaussian pulse, the solution of the Burgers equation is changed. Hence we apply DMD with different time intervals, and the result is shown in Figure 14b. We can see that at the bottom of the figure, two green dots are close to each other; this implies that the approximation of the eigenvalues from DMD is becoming inaccurate. Therefore, the time interval $t \in [100, 200]$ for the solution of the Burgers equation is not close enough to the simple invariant solution. Hence we can conclude that to obtain accurate DMD eigenvalues from the Burgers equation initially; we need to pick the time interval for the solution of the Burgers equation close to its simple invariant solution. However, there is no exact method to determine how "far away" the input data matrix $\mathbf{X}$ from the simple invariant solution for DMD, but we need to be as close as possible to the simple invariant solution to obtain the accurate result.

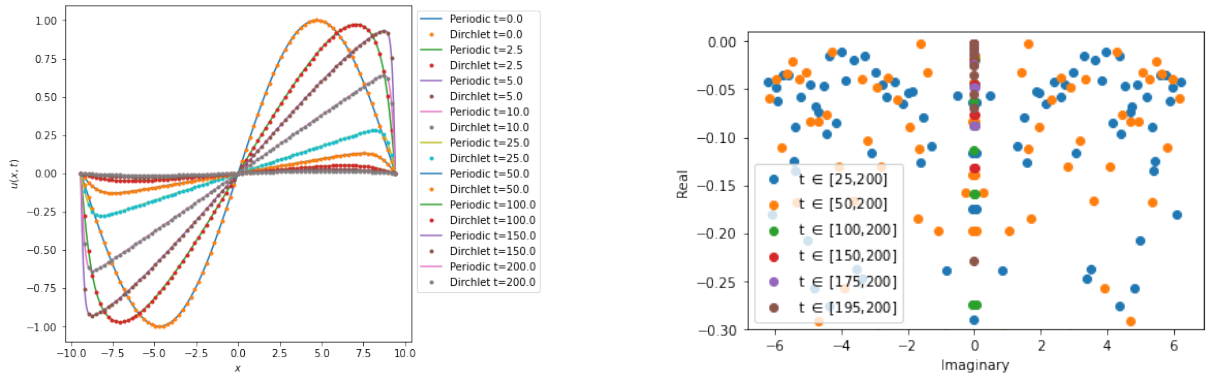

(a) (b)

Figure 14: (a): Evolution of $u_0(x) = \sin\left(\frac{2\pi x}{L}\right)$ for $t \leq 200$, The line is computed by periodic boundary condition, the dot is computed by Dirichlet boundary condition. (b): First a few eigenvalues from DMD of $u_0(x) = \exp[-(x + \left(\frac{\pi}{2}\right)^2)]$ with timestep $\Delta t = 0.5$, with the different time intervals between $25, 50, 100, 150, 175, 195$ to 200 for $\mathbf{g} = \mathbf{u}$ with periodic boundary condition.

6 Conclusions

In summary, the Koopman operator is linear and attractive, yet it is infinite dimensional even for system of ODEs. Alternatively, we can apply Koopman analysis to identify the key observable functions that evolve linearly with the flow of the dynamics rather than capture the evolution of all observable functions in appropriate function space. These special observables are called Koopman eigenfunction, which evolves exponentially in time. One of the main reasons we use the Koopman operator is that it can simplify the dynamics through the eigen-decomposition of the operator. Moreover, we have investigated that for a non-linear dynamical system, if it can be transformed into a linear dynamical system, and the eigenfunctions of the linear dynamical system become the basis of the Koopman observable functions, which forms a Koopman invariant subspace and span to form a finite-dimensional subspace of Hilbert space that contains the state. We explored the functionality of KMD by solving several examples of non-linear dynamical systems and studying the Burgers equation. We use Koopman invariant subspace to yield a finite-dimensional non-linear dynamical system to evolve any observables forward in time, as shown in Section 3.3.3.

In Chapter 4, we define the Exact DMD algorithm and use Python to implement the Algorithm 2. We use the same non-linear system as in Section 3.3.3 to examine the Exact DMD algorithm. We found that for a non-linear dynamical system with finitely many eigenvalues, there is a relationship between the largest absolute eigenvalue and the timestep Δt between the snapshot pairs that $\ln(\max\{|\lambda_i|\}\Delta t) \in [1, 10]$ reduces the error between the exact eigenvalues and DMD eigenvalues, as we have shown in Section 4.2.

In Chapter 5 we use numerical methods for Koopman Analysis on the Burgers equation with Dirichlet boundary condition via Cole-Hopf transformation to find the corresponding KMD for Burgers equation . We use finite difference methods to compare with the analytical solution to verify whether the analytical solution is correct and then use the analytical solution as the input of the DMD with two observables. In practice, we demonstrated the complete Koopman analysis of the Burgers equation with different boundary conditions to examine the DMD-Koopman operator connection. We find that for a small time interval, we use the linearised observable $\mathbf{g} = \mathbf{v}(\mathbf{u})$ to perform a better result than the observable $\mathbf{g} = \mathbf{u}$. We discussed that the input data matrix $\mathbf{X}$ should be how "far away" from the simple invariant solution to perform the first few matched DMD eigenvalues for different initial and boundary conditions.

Although we showed several results about apply Koopman mode analysis and DMD on non-linear systems and PDEs, there are still some limitations to this study. First, those results only work with a single fixed point non-linear system. Then, the DMD cannot handle the dynamic system that contains repeated exact eigenvalues, which results in the DMD giving out conjugate pair eigenvalues that do not match what we should have. Finally, it is extremely challenging to determine the suitable distance that "far away" to the simple invariant solutions.

As noted previously, we find the relationship between the largest absolute eigenvalue and the timestep between the snapshot pairs. However, this does not work with single fixed point non-linear systems containing infinitely many eigenvalues and multiple fixed point non-linear systems. An obvious next step would be to find the Koopman observable for the multiple fixed point system and determine how it can be related to some linear operator we know and then determine the parameters of DMD in the given non-linear system to perform a robust Koopman decomposition numerically. Furthermore, we only give a range of the distance from the simple invariant solution that starts badly but not the exact time. We may find a way to represent the distance from the simple invariant solution related to the error of the DMD and generalise it to all systems.

References

[1] E. Allen, J. Burns, D. Gilliam, J. Hill, and V. Shubov. The impact of finite precision arithmetic and sensitivity on the numerical solution of partial differential equations. *Mathematical and Computer Modelling*, 35(11):1165–1195, 2002.

[2] H. Arbabi. *Koopman spectral analysis and study of mixing in incompressible flows.* University of California, Santa Barbara, 2017.

[3] S. L. Brunton, B. W. Brunton, J. L. Proctor, and J. N. Kutz. Koopman invariant subspaces and finite linear representations of nonlinear dynamical systems for control. *PLOS ONE*, 11(2):1–19, 02 2016.

[4] S. L. Brunton, M. Budišić, E. Kaiser, and J. N. Kutz. Modern koopman theory for dynamical systems. *arXiv preprint arXiv:2102.12086*, 2021.

[5] J. Burgers. A mathematical model illustrating the theory of turbulence. volume 1 of *Advances in Applied Mechanics*, pages 171–199. Elsevier, 1948.

[6] J. D. Cole. On a quasi-linear parabolic equation occurring in aerodynamics. *Quarterly of Applied Mathematics*, 9(3):225–236, 1951.

[7] P. Gaspard, G. Nicolis, A. Provata, and S. Tasaki. Spectral signature of the pitchfork bifurcation: Liouville equation approach. *Phys. Rev. E*, 51:74–94, Jan 1995.

[8] D. M. Grobman. Homeomorphism of systems of differential equations. *Dokl. Akad. Nauk SSSR*, 128:880–881, 1959.

[9] P. Hartman. A lemma in the theory of structural stability of differential equations. 1960.

[10] P. Hartman. *Ordinary differential equations.* Classics in applied mathematics ; 38. Society for Industrial and Applied Mathematics SIAM, 2nd ed. edition, 2002.

[11] E. Hopf. The partial differential equation $u_t + uu_x = \nu u_{xx}$. *Communications on Pure and Applied Mathematics*, 3(3):201–230, 1950.

[12] N. D. Kazarinoff. Nonlinear oscillations, dynamical systems, and bifurcations of vector fields. *SIAM Review*, 26(4):600–601, 1984.

[13] B. O. Koopman. Hamiltonian systems and transformation in hilbert space. *Proceedings of the National Academy of Sciences*, 17(5):315–318, 1931.

[14] J. N. Kutz, S. L. Brunton, B. W. Brunton, and J. L. Proctor. *Dynamic mode decomposition: data-driven modeling of complex systems.* SIAM, 2016.

[15] I. Mezić. Spectral properties of dynamical systems, model reduction and decompositions. *Nonlinear Dynamics*, 41:309–325, 08 2005.

[16] I. Mezić. Analysis of fluid flows via spectral properties of the koopman operator. *Annual Review of Fluid Mechanics*, 45(1):357–378, 2013.

[17] I. Mezić. Spectrum of the koopman operator, spectral expansions in functional spaces, and state space geometry, 2017.

[18] I. Mezić and A. Banaszuk. Comparison of systems with complex behavior. *Physica D: Nonlinear Phenomena*, 197(1):101–133, 2004.

[19] J. Page. Applied dynamics system. *University of Edinburgh*, 2022.

[20] J. Page and R. R. Kerswell. Koopman analysis of burgers equation. *Phys. Rev. Fluids*, 3:071901, Jul 2018.

[21] C. W. Rowley, I. Mezić, S. Bagheri, P. Schlatter, and D. S. Henningson. Spectral analysis of nonlinear flows. *Journal of Fluid Mechanics*, 641:115–127, 2009.

[22] P. J. Schmid. Dynamic mode decomposition of numerical and experimental data. *Journal of fluid mechanics*, 656:5–28, 2010.

[23] K. Taira, S. L. Brunton, S. T. M. Dawson, C. W. Rowley, T. Colonius, B. J. McKeon, O. T. Schmidt, S. Gordeyev, V. Theofilis, and L. S. Ukeiley. Modal analysis of fluid flows: An overview. *AIAA Journal*, 55(12):4013–4041, 2017.

[24] J. H. Tu, C. W. Rowley, D. M. Luchtenburg, S. L. Brunton, and J. N. Kutz. On dynamic mode decomposition: Theory and applications. *Journal of Computational Dynamics*, 1(2):391–421, 2014.